AFRL-RV-HA-TR-2010-1026

Communications/Navigation Outage Forecasting System (C/NOFS)

Laila Jeong

Final Report

21 Feb 2010

AIR FORCE RESEARCH LABORATORY
Space Vehicles Directorate
29 Randolph Road
AIR FORCE MATERIEL COMMAND
Hanscom AFB, MA 01731-3010

AFRL-RV-HA-TR-2010-1026

This technical report has been reviewed and is approved for publication.

/ signed /
Robert A Morris, Chief
Battlespace Environment Division

/ signed /
Laila Jeong
Research Chemist

/ signed /
Dwight T. Decker, Chief
Space Weather Center of Excellence

REPORT DOCUMENTATION PAGE

Form Approved
OMB No. 0704-01-0188

PLEASE DO NOT RETURN YOUR FORM TO THE ABOVE ADDRESS.

1. REPORT DATE *(DD-MM-YYYY)*	2. REPORT TYPE	3. DATES COVERED *(From - To)*
11-02-2010	Scientific, Final	1 Oct 2001 – 30 Sep 2009

4. TITLE AND SUBTITLE

Communications/Navigation Outage Forecasting System (C/NOFS)

5a. CONTRACT NUMBER

5b. GRANT NUMBER

5c. PROGRAM ELEMENT NUMBER
621010F

6. AUTHORS
Laila Jeong

5d. PROJECT NUMBER
1010

5e. TASK NUMBER
CN

5f. WORK UNIT NUMBER
ZZ

7. PERFORMING ORGANIZATION NAME(S) AND ADDRESS(ES)

Air Force Research Laboratory /RVB
29 Randolph Road
Hanscom AFB, MA 01731-3010

8. PERFORMING ORGANIZATION REPORT NUMBER
AFRL-VS-HA-TR-2010-1026

9. SPONSORING/MONITORING AGENCY NAME(S) AND ADDRESS(ES)

10. SPONSOR/MONITOR'S ACRONYM(S)

11. SPONSOR/MONITOR'S REPORT NUMBER(S)

12. DISTRIBUTION/AVAILABILITY STATEMENT
Approved for Public Release; distribution unlimited.

13. SUPPLEMENTARY NOTES

14. ABSTRACT

The Communications/Navigation Outage Forecasting System (C/NOFS) satellite was successfully launched in April 2008 into a low earth orbit. It has a six instrument payload for monitoring and forecasting the ionosphere. The satellite observations are combined with other data and modeling results to characterize ionospheric irregularities that are likely to produce scintillation.

15. SUBJECT TERMS
Ionospheric scintillation
Equatorial plasma bubbles
Ionospheric spread F

16. SECURITY CLASSIFICATION OF:			17. LIMITATION OF ABSTRACT	18. NUMBER OF PAGES	19a. NAME OF RESPONSIBLE PERSON
a. REPORT	b. ABSTRACT	c. THIS PAGE			Laila Jeong
UNCL	UNCL	UNCL	UNL	24	19B. TELEPHONE NUMBER *(Include area code)*

Contents

Communication/Navigation Outage Forecasting System (C/NOFS)

The goal of the Communication/Navigation Outage Forecasting System (C/NOFS) is to specify and forecast the equatorial ionosphere, including spread F and ionospheric scintillation. Scintillation is a random fluctuation in signal phase and amplitude that develops when radio waves pass through ionospheric electron density irregularities. Irregularities that cause the most intense scintillation occur naturally, after sunset, within a ±20° band of latitude around the magnetic equator. Although the statistical occurrence of scintillation is relatively well known with respect to location, time of day and solar cycle, the night-to-night variability is much more difficult to forecast.

In order to develop the capability to forecast the onset of ionospheric irregularities that trigger scintillation, the C/NOFS satellite was specifically designed with a six instrument payload for making in situ and remote sensing measurements of the ionosphere. The C/NOFS satellite was successfully launched in April 2008 into a low earth orbit at 13° inclination. C/NOFS is the first satellite dedicated to monitoring and forecasting ionospheric conditions. The instruments measure electric fields, plasma characteristics, neutral winds, and the strength of scintillation-producing irregularities. Various models and analysis tools use the spacecraft observations and combine them with ground-based and other satellite data to characterize ionospheric irregularities that are likely to produce scintillation.

The six instruments on the C/NOFS satellite are as follows:

CERTO - Coherent Electromagnetic Radio Tomography

- Built by Naval Research Laboratory (NRL)
- Consists of a beacon and antenna that transmit at three frequencies to ground receivers
- The signals measured by the ground receivers are analyzed to determine the amount of scintillation along the path between the C/NOFS satellite and the ground receiver
- If the signals are not distorted, then there is no scintillation. The more distorted the signals are, the more intense the scintillation is.
- The data measured by CERTO are used to validate and improve physics models developed by AFRL/RV to forecast scintillation

CORISS - C/NOFS Occultation Receiver for Ionospheric Sensing and Specification

- Built by Aerospace Corporation
- Consists of a specially-designed Global Positioning System (GPS) receiver and antenna for remote sensing of the ionosphere
- It measures signals transmitted by the global constellation of GPS satellites
- The signals are analyzed to determine the number of charged particles along the path between the GPS satellite and the C/NOFS satellite
- The number of charged particles in disturbed regions of the ionosphere vary depending on the severity of the scintillations.

- The data measured by the CORISS instrument are used as inputs to validate and improve physics models developed by AFRL/RV to forecast scintillation

IVM - Ion Velocity Meter

- Built by University of Texas at Dallas (UTD)
- Consists of two sensors:
    - one sensor has a square opening and measures the speed and direction of charged particles that are moving perpendicular to the C/NOFS satellite's direction of motion
    - the other sensor has a round opening and measures the speed and direction of charged particles that are moving along the satellite's orbit track. This sensor also measures the number of charged particles in the region of the ionosphere that the C/NOFS satellite is flying through
- The speed and direction of charged particles in disturbed regions of the ionosphere are important indicators of whether or not scintillation will occur
- The data measured by the IVM instrument are used as inputs to validate and improve physics models developed by AFRL/RV to forecast scintillation.

NWM - Neutral Wind Meter

- Built by University of Texas at Dallas (UTD)
- Consists of two sensors. One sensor measures the speed and direction of the gas (uncharged particles) flowing in the ionosphere in the direction of the satellite's motion and the other sensor measures the gas flow perpendicular to the satellite's track.
- The motion of the gas affects the distribution of charged particles in the ionosphere. When the gas flow produces an irregular distribution of charged particles then there is a higher probability that scintillation will occur.
- The data measured by the NWM instrument are used as inputs to validate and improve physics models developed by AFRL/RV to forecast scintillation.

PLP - Planar Langmuir Probe

- Built by Air Force Research Laboratory, Space Vehicles Directorate (AFRL/RV)
- It measures the number of charged particles along the path of the satellite
- As the satellite is moving, the PLP instrument sweeps up charged particles in its path much like a butterfly net stuck out of the window of a moving car would sweep up mosquitoes.
- When the charged particles hit the metal plate at the front of the instrument they create an electrical current signal. The signal is measured and analyzed to determine the number of charged particles.
- When the ionosphere is undisturbed, the PLP instrument measures a smoothly varying signal along the orbital track. However, when the ionosphere is disturbed, the signals measured by PLP are rapidly fluctuating.
- The PLP signal fluctuations are an indicator of scintillation. The more rapid the signal fluctuations, the more intense the scintillation is.

- The PLP data are used in models to specify exactly where scintillations are at the time of the measurement. This is referred to as nowcasting. The data are also used to validate and improve physics models developed by AFRL/RV to forecast scintillation.

VEFI - Vector Electric Field Instrument

- Built by National Aeronautics and Space Administration/Goddard Space Fight Center (NASA/GSFC)
- Consists of six booms, each 10 m long, at the end of which are sensors.
- The six sensors (one per boom) measure the force that exists in a region between particles that have opposite charges. This quantity is called the electric field and the VEFI instrument measures both the strength and direction of this field.
- The electric field in the ionosphere is important because it sets in motion the charged particles. These motions can cause the ionosphere to become disturbed and unstable, thereby producing scintillations.
- Changes in the electric field over time are an indicator of future scintillation.
- The data measured by the VEFI instrument are used as inputs to validate and improve physics models developed by AFRL/RV to forecast scintillation.

The data collected by the C/NOFS satellite are unprecedented in ionospheric research. The scientific papers included in this report represent the large breadth and depth of the satellite measurements and their analysis. Among the new findings are broad plasma density decreases of up to an order of magnitude for a few months around the June solstice that are believed to be due to cooling of the ionosphere and thermosphere during these times. A very surprising discovery made from the C/NOFS measurements is deep plasma depletions at sunrise that appear to be associated with upward plasma drifts. The AFRL physics-based model PBMOD was used extensively to make comparisons with satellite data. The model was found to successfully reproduce density depletions observed at early morning local times during four consecutive orbits of the satellite. In addition, the model was found to reproduce the observed latitudinal and longitudinal scale sizes of the plasma depletions. In another unique finding, the C/NOFS satellite captured data during a high speed stream (HSS) event in which the ionosphere went from quiescent to disturbed. During this event, post-midnight irregularities included strong equatorial plasma bubbles.

Broad plasma decreases in the equatorial ionosphere

Cheryl Y. Huang,[1] Frank A. Marcos,[1] Patrick A. Roddy,[1] Marc R. Hairston,[2] W. Robin Coley,[2] Christopher Roth,[3] Sean Bruinsma,[4] and Donald E. Hunton[1]

Received 2 June 2009; accepted 23 June 2009; published 6 August 2009.

[1] During June 2008 broad plasma density decreases (BPDs) were detected repeatedly by the Planar Langmuir Probe (PLP) on board the Communication/Navigation Outage Forecasting System (C/NOFS) satellite. These density minima, not to be confused with Equatorial Plasma Bubbles (EPBs), occurred within 15° of the equator, consisted of reductions in plasma density up to an order of magnitude and extended across several degrees in azimuth along the orbit. Analysis revealed that the BPDs occurred nearly daily from May through July 2008 on C/NOFS, and that the widest BPDs were observed in the vicinity of the South Atlantic Anomaly (SAA). Similar BPDs simultaneous with the C/NOFS measurements were observed by instruments on the CHAllenging Minisatellite Payload (CHAMP) and Defense Meteorological Satellite Program (DMSP) satellites. An examination of plasma densities observed by the DMSP satellites over several years revealed that these phenomena were a frequent occurrence during (1) the period around June solstices; during (2) solar minimum years; (3) in the vicinity of the SAA. Neutral densities were examined during periods when BPDs were detected, and at times there are simultaneous neutral depletions. One possible explanation is a decrease in temperature of both ions and neutrals in the equatorial region at these times, consistent with downwelling in the ionosphere and thermosphere. Measurements of plasma temperatures on DMSP support this hypothesis.
Citation: Huang, C. Y., F. A. Marcos, P. A. Roddy, M. R. Hairston, W. R. Coley, C. Roth, S. Bruinsma, and D. E. Hunton (2009), Broad plasma decreases in the equatorial ionosphere, *Geophys. Res. Lett.*, *36*, L00C04, doi:10.1029/2009GL039423.

1. Introduction

[2] Between May and August 2008, the Planar Langmuir Probe (PLP) on the C/NOFS satellite regularly measured reduced plasma density on the nightside in the equatorial region lasting several minutes and occurring over a broad range of longitudes. Density within the depleted region was reduced by up to an order of magnitude below the density outside the Broad Plasma Decrease (BPD). The June 2008 solstice occurred during an extremely quiet solar minimum interval. The minimum Disturbance Storm Time (Dst) index value during the month was −40 nT and this occurred on 15 June. There are several periods when the Auroral Electrojet (AE) index reaches 1000 nT, but these do not correlate with the nearly daily occurrences of BPDs.

[3] Densities on the DMSP satellites were examined for the same interval, and BPDs were noted at or near equatorial latitudes. The deepest BPDs were observed close to the SAA which encompasses the entire azimuthal area from the west coast of South America to the center of southern Africa and from the geographic equator to 50° S. Density depletions were observed on DMSP up to 40% below the ambient density outside the depleted area.

[4] We have studied these depletions using a large array of satellite-based observations of the ionosphere-thermosphere (IT) system in order to determine their climatology. This report briefly summarizes the results of our study of IT observations and our interpretation of these observations.

2. Instrumentation

[5] The PLP on C/NOFS measures plasma densities, electron temperatures and density fluctuations at rates ranging from 32 to 1024 samples per second. In this paper we focus on electron densities on the nightside. During the period in this study, 17–19 June 2008, the satellite altitude when depletions were observed varied from 400 to 600 km, with the bulk of measurements made between 400 and 500 km.

[6] Density measurements on DMSP were made by the Special Sensors-Ions, Electrons, and Scintillation (SSIES) suite. The measurements used in this study come from SSIES-3 flown on DMSP F16. We use output from the Retarding Potential Analyzer (RPA) which gives plasma densities and temperatures every 1 s, over the range 10^2–10^6 cm^{-3} with an accuracy of 10%.

[7] Plasma densities on the CHAMP satellite were obtained from the PLP [*Cooke et al.*, 2003; *Roth*, 2004], which monitors the spacecraft potential, ion density, and electron temperature. A one-second sweep is performed every 15 seconds. Neutral densities were measured by the STAR accelerometer [*Bruinsma et al.*, 2004] every 10 seconds.

[8] Neutral densities on the Gravity Recovery and Climate Experiment (GRACE) satellite were measured using super-STAR accelerometers, similar to the STAR accelerometer on CHAMP, [*Cheng et al.*, 2008] with a precision an order of magnitude greater than the CHAMP instrument. In this study, 5-second averaged data were used.

3. Observations

[9] An example of the observations which triggered this investigation is shown in Figure 1. In Figure 1a, shown is

[1]Space Vehicles Directorate, Air Force Research Laboratory, Hanscom AFB, Bedford, Massachusetts, USA.
[2]William B. Hanson Center for Space Sciences, University of Texas at Dallas, Richardson, Texas, USA.
[3]Atmospheric and Environmental Research, Inc., Lexington, Massachusetts, USA.
[4]Centre National d'Etudes Spatiales, Toulouse, France.

0094-8276/09/2009GL039423$05.00

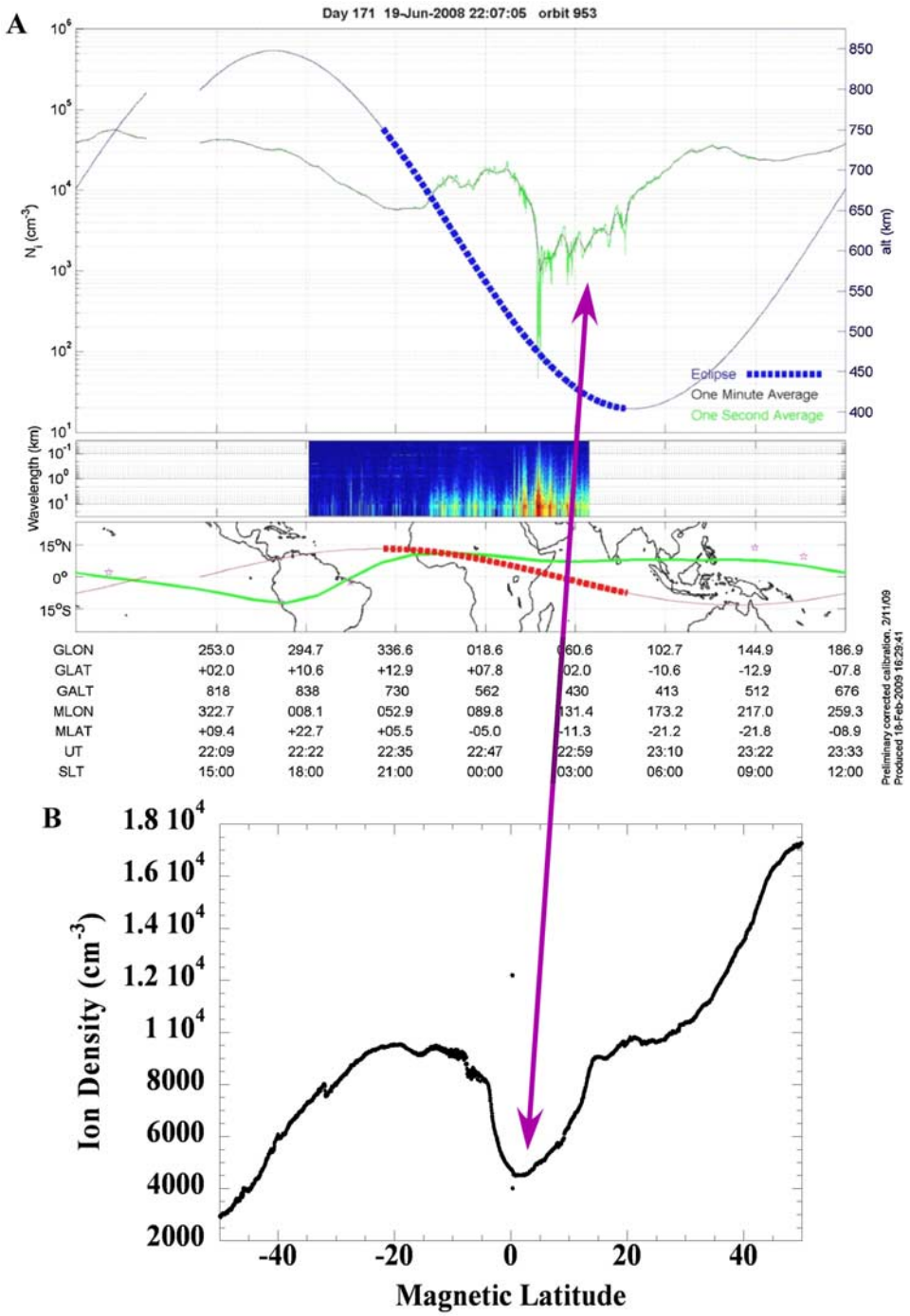

Figure 1. C/NOFS and DMSP observations of a Broad Plasma Depletion (BPD) on 19 June 2008. (a, top) Plasma density (black line) in 1-minute resolution, as well as 1-second resolution (green line). C/NOFS altitude is indicated by the blue line, with the heavy dotted section showing when the satellite is in darkness. (middle) Spectrum of the high-time resolution density fluctuations. (bottom) The magnetic equator is shown by a green trace, and satellite orbit is indicated by the red trace, with the heavy dotted section indicating when the spacecraft is in darkness. The BPD (purple arrow) starts at 2253 UT, with recovery after 2310 UT. (b) In the DMSP F16 plot the ion density is plotted as a function of magnetic latitude during an equatorial crossing at 2236 UT. The BPD (purple arrow) occurs at the equator as indicated.

the PLP plot from C/NOFS on 19 June 2008. In Figure 1a (top), plasma density is indicated by the black trace which shows 1-minute averaged data. 1-second data are illustrated by the green trace. Also shown is the satellite altitude in blue with the heavy dotted line indicating when the spacecraft is in darkness. In Figure 1a (middle), the color spectrogram shows the frequency of the density fluctuations. Figure 1a (bottom) shows the orbit of the satellite in red, the heavy dotted segment showing when C/NOFS is in darkness. The magnetic equator is plotted in green.

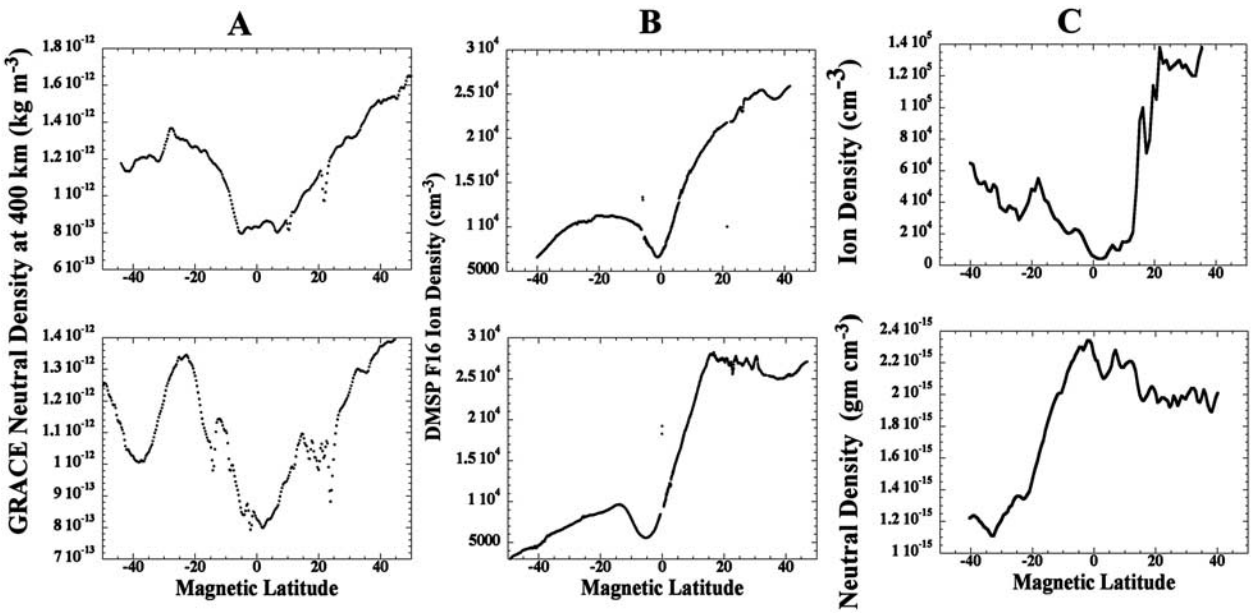

Figure 2. (a) Two consecutive nightside orbits of GRACE on 9 June 2005. (top) The first crossing occurred at 2200 UT, 20.3 MLT, 329°E. long. (geog.), altitude of 468 km; (bottom) the second at 2333 UT, 20.2 MLT, 305°E. long. (geog.), 470 km altitude. (b) DMSP F16 equatorial crossings on the same day. (top) The crossing at 2114 UT, 20.5 MLT, 343°E. long. (geog.); (bottom) the plasma density at 2253 UT, 20.6 MLT, 320°E. long. (geog.). Reduced neutral and plasma densities in all four plots can be clearly seen. (c) CHAMP ion and neutral densities at 2224 UT, 17 June 2008. Satellite location is 1.23 MLT, 329 km altitude, 40°E long. (geog.) (top) The plasma density is shown, as a function of latitude. (bottom) CHAMP Neutral density.

[10] At approximately 2253 UT, at an altitude of about 475 km, and at 40° E geog. long., the plasma density decreases sharply as illustrated by the black trace. Densities gradually recover, and are at their pre-depleted level by 2310 UT. The magnetic latitude of the plasma decrease varies from −8° to −21°. In 1B, below, is shown the DMSP F16 plot of plasma densities for the equatorial crossing at 2236 UT. The orbit corresponds to a single crossing of the eveningside equatorial ionosphere at an altitude of 840 km, and magnetic local time (MLT) of 20.2. Note that while the C/NOFS and DMSP measurements are nearly simultaneous, there is considerable spatial separation between the two satellites. The magnetic equator is placed at the center of the plot, and latitudes from −50° S to 50° N are shown in intervals of 10°. Indicated by the arrow, there is a large reduction in plasma density in the equator at 2236 UT, at 318° E geographic longitude (geog. long.), corresponding to the SAA.

[11] Accurate statistics for C/NOFS cannot be obtained due to the orbital variations in altitude, latitude and longitude during the May–July 2008 interval. However in this period, barring data gaps, on all but 8 days BPDs were observed by the PLP. On most days, BPDs were seen on multiple orbits if the satellite was in the vicinity of the SAA on the nightside.

[12] As can be seen in Figure 1, the extent of the depleted region is large. In the C/NOFS plot, the area exceeds 60° in longitude and 15° in latitude. The DMSP depletion is more than 15° in latitude. For this reason, we are careful to describe these as broad plasma density decreases (BPDs), not to be confused with EPBs which are orders of magnitude smaller in spatial extent. However there is a relation between BPDs and EPBs. BPDs generally originate over the SAA, and are relatively shallow and unstructured. Over subsequent orbits of C/NOFS, they migrate eastward, and the depletion becomes narrower and deeper. When the BPD reaches the dawn meridian, they are considerably narrower with very deep structures within the BPD. For more detail, we refer the reader to *de la Beaujardière et al.* [2009].

[13] Having confirmed the presence of BPDs on DMSP in June 2008, we examined its extensive database for other examples. We found that BPDs occur regularly on the nightside in (1) June solstices which occur (2) during solar minima, (3) predominantly in the SAA. During the period from 1 May–31 July 2008, BPDs were observed on DMSP F16 on 87 of the 92 days. In addition, during intervals centered on the June solstices of 1995, 1996, 2005, 2006 and 2007 we found BPDs on DMSP repeatedly.

[14] Neutral densities were also examined for possible connection with the BPDs. CHAMP and GRACE accelerometer data were studied for the periods when large BPDs were recorded. Examples of neutral density decreases observed on GRACE are shown in Figure 2a. On 9 June 2005, two successive nightside orbits are shown. In Figure 2a (top), the equatorial crossing occurred at 22 UT, at a location of 20.3 MLT, altitude of 468 km, 329° E geog. long. In Figure 2a (bottom), the equatorial crossing occurred at 2333 UT, at 20.2 MLT and 470 km altitude, 305°E geog. long. In both orbits, reductions in neutral density up to 45% can be seen around the equator. The other 12 equatorial

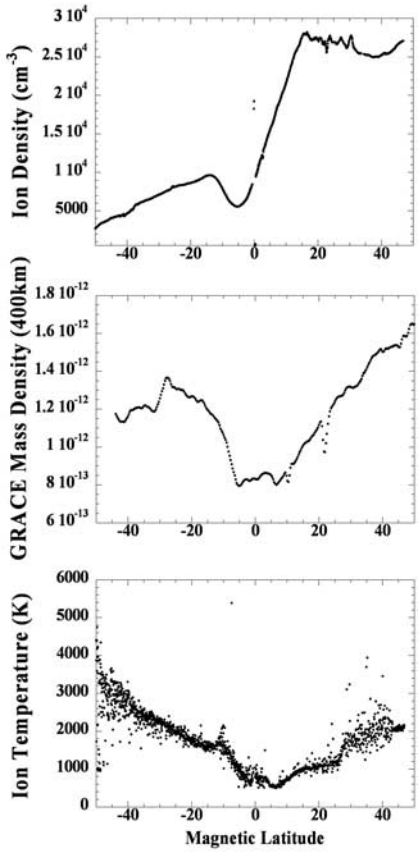

Figure 3. (top) Plasma density and (bottom) temperature from DMSP F16 on 9 June 2005, with (middle) GRACE neutral density. Plasma and neutral densities are both reduced in the equatorial region. Lower temperatures at the equator clearly indicate cooling at this time.

crossings on this day which do not occur close to the SAA do not display this phenomenon.

[15] In Figure 2b are shown two equatorial crossings made by DMSP F16 on the same day. Figure 2b (top) shows measurements made at 2114 UT, at a 343°E geog. long., and 20.5 MLT. Figure 2b (bottom) shows the subsequent crossing at 2253 UT, 320°E geog. long., and 20.6 MLT. These crossings are nearly coincident both in time and space with the GRACE equatorial orbits on the left side of Figure 2. The density reductions inside the BPDs on DMSP are approximately 40% of ambient values.

[16] On 17 June 2008, on three consecutive equatorial crossings between 2048 and 2400 UT, the PLP on CHAMP detected deep BPDs. The CHAMP orbit crossed C/NOFS at 2355 UT which observed highly structured BPDs at this time. During the 2224 UT crossing, second of the three, CHAMP was located at 329 km altitude, 1.23 MLT, 40°E geog. long. In Figure 2c are shown the ion and neutral densities during this crossing. The PLP densities show a BPD which is over 30° across in latitude, with a plasma density that is more than an order of magnitude below ambient values. The neutral density decrease is about 10% below the densities outside the neutral depletion. It is not clear whether the difference between this example and that shown in Figure 2a is due to the significantly lower neutral densities during 2008, or if this represents a difference in the phenomenology.

4. Discussion

[17] The appearance of BPDs can be explained in several ways. For a number of reasons we rule out the possibility of EPBs as the cause. The climatology of EPBs is in conflict with the climatology of the BPDs [*Gentile et al.*, 2006]. During solar minimum, there are few EPBs which reach DMSP altitude, and during June EPB occurrence in the SAA region is low [*Huang et al.*, 2002]. During times of maximum occurrence of EPBs during the December solstices and equinoxes, BPDs have not been detected. As already mentioned, the size of BPDs exceeds normal EPBs by a large factor.

[18] A second possible cause of BPDs and neutral depletions is a change in chemistry in the ionosphere and thermosphere. This occurs during magnetic storms, when large changes in IT densities occur [*Crowley et al.*, 2006]. Other systemic variations in the thermosphere occur as a result of global warming [*Akmaev et al.*, 2006]. However neither of these mechanisms can account for the specific climatology associated with the BPDs, nor the simultaneous decreases in neutral and ion densities in the equatorial region.

[19] Coincident reductions in neutral and plasma densities narrow the range of possible causes. Simultaneous ion and neutral density reductions have been observed in EPBs [*Bencze et al.*, 2000] but as we have pointed out, these BPDs cannot be bubbles. The minima in ion and neutral densities can be described by a change in the topside scale height, defined as $H = kT/mg$ where k is Boltzmann's constant, T is the temperature of the species, m the mass of the species and g the gravitational constant [*Rishbeth and Garriott*, 1969].

[20] A change in plasma and neutral density can be due to a change in T, the plasma or neutral temperature, or m, the mass of the species, or both. An examination of the fraction of light ions (H^+) during the DMSP observations shows that during the June 2005 events, this fraction is less than 50% in the minimum of the BPD, and the opposite is true during June 2008, when the solar cycle is in a deep minimum. This rules out a persistent change in ion composition.

[21] We suggest that the most likely explanation is a cooling or downwelling of the equatorial region during these periods. This would account for simultaneous decreases in both neutrals and plasma density. To verify this hypothesis, we examined ion temperatures (T_i) on DMSP during the periods when BPDs were seen. In Figure 3 (bottom), we show T_i obtained from DMSP F16 during the 2253 UT equatorial crossing on 9 June 2005, together with ion density (Figure 3, top) measured simultaneously and the GRACE neutral density (Figure 3, middle) from the 2333 UT crossing. There is a clear decrease in T_i at the equator of approximately 50% to a minimum value of 547K. This is comparable in spatial extent with the BPD noted on DMSP and the neutral depletion on GRACE. Similar variations in T_i occur during the 2114 UT crossing.

[22] During 2008 the plasma density in the BPD is reduced to such an extent, and the percentage of light ions so high, that accurate values of T_i cannot be obtained

reliably. However up to the point where the uncertainty in T_i becomes large, the temperatures are clearly decreasing. This is true of both DMSP and C/NOFS.

[23] T_i measured on DMSP F16 in the BPDs is lower than values reported during other nighttime solar minimum conditions when T_e was approximately 600–700K over the Indian sector [*Bhuyan et al.*, 2002]. They are also lower than values predicted by the International Reference Ionosphere (IRI) model [*Gulyaeva and Titheridge*, 2006] run for these periods (June 2005 and June 2008) and approximate location (330°E longitude). These model values are approximately 1000K. We believe that the discrepancy between our results and past studies is due to the localized nature of BPDs, both in time and space. Variability in ion and electron densities and temperatures have been noted in previous studies [*Forbes et al.*, 2000; *Gulyaeva and Titheridge*, 2006] but no consistent study of density variations as functions of (1) solar cycle, (2) season, and (3) location has been undertaken until now.

5. Summary

[24] We have presented observations of BPDs and neutral density depletions which occur during June solstices, near the equator during solar minimum years. These observations were made from altitudes of 330 km to 840 km using several different detectors flown on a number of spacecraft. The appearance of simultaneous neutral density depletions in the equatorial region narrows the range of explanations to cooling or downwelling of the ionosphere and thermosphere during these times. This hypothesis is supported by direct measurements of plasma temperature, which also show minima in the equatorial region, well below the predicted values based on the IRI model or other observations. At present no mechanism has been proposed which accounts for the basic formation of BPDs or their climatology.

[25] **Acknowledgments.** The C/NOFS mission is supported by the Air Force Research Laboratory, the Department of Defense Space Test Program, the National Aeronautics and Space Administration, the Naval Research Laboratory, and the Aerospace Corporation. DMSP data were made available through funding by the DMSP program office. We thank J. Retterer for the IRI model results. This research was supported by Air Force Office of Scientific Research Task 2301SDA5, and Air Force contract FA8718-05-C-0036 with Atmospheric and Environmental Research Inc. Research at the University of Texas at Dallas was supported by the National Aeronautics and Space Administration under contract NAS5-01068.

References

Akmaev, R. A., V. I. Fomichev, and X. Zhu (2006), Impact of middle-atmospheric composition changes on greenhouse cooling in the upper atmosphere, *J. Atmos. Sol. Terr. Phys.*, *68*, 1879–1889, doi:10.1016/j.jastp.2006.03.008.

Bencze, P., I. Almar, and E. Illes-Almar (2000), Further results referring to the neutral density depletions attributed to plasma bubbles, *J. Atmos. Sol. Terr. Phys.*, *62*, 1339–1350, doi:10.1016/S1364-6826(00)00149-8.

Bhuyan, P. K., M. Chamua, P. Subrahmanyam, and S. C. Garg (2002), Diurnal, seasonal and latitudinal variations of electron temperature measured by the SROSS C2 satellite at 500 km altitude and comparison with the IRI, *Ann. Geophys.*, *20*, 807–815.

Bruinsma, S., D. Tamagnan, and R. Biancale (2004), Atmospheric densities derived from CHAMP/STAR accelerometer observations, *Planet. Space Sci.*, *52*, 297–312, doi:10.1016/j.pss.2003.11.004.

Cheng, M.-K., B. D. Tapley, S. Bettadpur, and J.C. Ries (2008), Thermospheric density from analysis of 6-year GRACE accelerometer Data, paper presented at the AIAA/AAS Astrodynamics Specialist Conference and Exhibit, Am. Inst. of Aeronaut. and Astronaut., Honolulu, Hawaii.

Cooke, D., W. Turnbull, C. Roth, A. Morgan, and R. Redus (2003), Ion drift-meter status and calibration, in *First CHAMP Mission Results for Gravity, Magnetic, and Atmospheric Studies*, edited by C. Reigber, H. Lühr, and P. Schwintzer, pp. 212–219, Springer, Berlin.

Crowley, G., et al. (2006), Global thermosphere-ionosphere response to onset of November 20, 2003 magnetic storm, *J. Geophys. Res.*, *111*, A10S18, doi:10.1029/2005JA011518.

de La Beaujardière, O., et al. (2009), C/NOFS observations of deep plasma depletions at dawn, *Geophys. Res. Lett.*, doi:10.1029/2009GL038884, in press.

Forbes, J. M., S. E. Palo, and X. Zhang (2000), Variability of the ionosphere, *J. Atmos. Sol. Terr. Phys.*, *62*, 685–693, doi:10.1016/S1364-6826(00)00029-8.

Gentile, L. C., W. J. Burke, and F. J. Rich (2006), A global climatology for equatorial plasma bubbles in the topside ionosphere, *Ann. Geophys.*, *24*, 163–172.

Gulyaeva, T. L., and J. E. Titheridge (2006), Advanced specification of electron density and temperature in the IRI ionosphere–plasmasphere model, *Adv. Space Res.*, *38*, 2587–2595, doi:10.1016/j.asr.2005.08.045.

Huang, C. Y., W. J. Burke, J. S. Machuzak, L. C. Gentile, and P. J. Sultan (2002), Equatorial plasma bubbles observed by DMSP satellites during a full solar cycle: Toward a global climatology, *J. Geophys. Res.*, *107*(A12), 1434, doi:10.1029/2002JA009452.

Rishbeth, H., and O. K. Garriott (1969), *Introduction to Ionospheric Physics*, Academic, New York.

Roth, C. J. (2004), DIDM-2 sensor commanding, data collection, processing and analysis, *Rep. AFRL-VS-HA-TR-2004-1204*, Air Force Res. Lab., Hanscom AFB, Mass.

S. Bruinsma, Centre National d'Etudes Spatiales, 18, Avenue E. Belin, F-31401 Toulouse CEDEX, France.

W. R. Coley and M. R. Hairston, William B. Hanson Center for Space Sciences, University of Texas at Dallas, P.O. Box 830688 WT15, Richardson, TX 75083-0688, USA.

C. Y. Huang, D. E. Hunton, F. A. Marcos, and P. A. Roddy, Space Vehicles Directorate, Air Force Research Laboratory, 29 Randolph Road, Hanscom AFB, MA 01731-3010, USA. (afrl.rvb.pa@hanscom.af.mil)

C. Roth, Atmospheric and Environmental Research, Inc., 131 Hartwell Avenue, Lexington, MA 02421-3136, USA.

C/NOFS observations of plasma density and electric field irregularities at post-midnight local times

W. J. Burke,[1] O. de La Beaujardière,[1] L. C. Gentile,[1] D. E. Hunton,[1] R. F. Pfaff,[2] P. A. Roddy,[1] Y.-J. Su,[1] and G. R. Wilson[1]

Received 11 May 2009; revised 1 July 2009; accepted 13 July 2009; published 19 September 2009.

[1] We report on plasma densities and electric fields measured by the C/NOFS satellite between 10 and 20 June 2008. Midway through the interval, geomagnetic conditions changed from quiescent to disturbed as a high speed stream (HSS) in the solar wind passed Earth. During the HSS passage C/NOFS encountered post-midnight irregularities that ranged from strong equatorial plasma bubbles to longitudinally broad depletions. At the leading edge of the HSS the interplanetary magnetic field rapidly intensified and rotated causing auroral electrojet currents to rise and fall within a few hours. As the electrojet relaxed, C/NOFS witnessed a rapid transition from a weakly to a strongly disturbed equatorial ionosphere that lasted ~10 hours. Eastward polarization electric fields intensified within locally depleted flux tubes. We discuss relative contributions of gravity-driven currents, overshielding electric fields and disturbance dynamos as drivers of post-midnight depletions.
Citation: Burke, W. J., O. de La Beaujardière, L. C. Gentile, D. E. Hunton, R. F. Pfaff, P. A. Roddy, Y.-J. Su, and G. R. Wilson (2009), C/NOFS observations of plasma density and electric field irregularities at post-midnight local times, *Geophys. Res. Lett.*, *36*, L00C09, doi:10.1029/2009GL038879.

1. Introduction

[2] Electromechanical forces that couple the magnetosphere-ionosphere-thermosphere (MIT) system can cause intense plasma density (δN_i) irregularities to grow in the low-latitude ionosphere. To improve understanding of irregularity formation, the Communication/Navigation Outage Forecasting System (C/NOFS) satellite was launched on 16 April 2008 into a 13° inclined orbit with apogee and perigee at ~850 and 400 km, respectively. *de La Beaujardière and C/NOFS Science Definition Team* [2003] described the mission's goals and the scientific payload designed to attain them. Here we examine δN_i variations sampled by the Planar Langmuir Probe (PLP) on C/NOFS during the solar minimum period 10–20 June 2008 when perigee was on the nightside.

[3] A striking, new feature of C/NOFS observations is the detection of deep plasma depletions at topside altitudes after local midnight. Reported irregularities appear as: (1) local depletions called equatorial plasma bubbles (EPBs) and (2) longitudinally broad, depletions that we call "plasma trenches." EPBs are magnetically field-aligned, with typical east-west dimensions of ~100 km [*Basu*, 1997] and are usually found at evening local times (LTs). Reported satellite detections of post-midnight EPBs are relatively rare [*Burke*, 1979]. Longitudinally broad (>500 km) depletions develop in the evening sector during the main phases of large magnetic storms when the peak of the F-layer rises above the spacecraft [*Greenspan et al.*, 1991]. C/NOFS has detected similar phenomena at post-midnight local times under much less stressful geomagnetic conditions.

[4] EPBs begin as small-amplitude irregularities at bottomside altitudes then intensify via a generalized Rayleigh-Taylor (R-T) instability [*Balsley et al.*, 1972; *Ott*, 1978]. Forces driving the R-T instability include gravity-driven currents [*Eccles*, 2004] and quasi-DC electric fields ($\mathbf{E_0}$) with eastward components. The main sources of eastward components in the dusk sector are: (1) solar quiet (*Sq*) current system interactions with conductivity gradients near sunset, and (2) penetration electric fields from high latitudes. Polarization electric fields (E_P) can be much larger than E_0, allowing bubbles to percolate through the topside at high speeds. Inside trenches E_0 may dominate. Our analysis utilizes simultaneous measurements of plasma densities by the planar Langmuir probe (PLP) and the Vector Electric Field Instrument (VEFI) [*de La Beaujardière and C/NOFS Science Definition Team*, 2003] observed in and near irregularities. VEFI measures the total electric field's east-west (E_{zonal}) component that includes E_0 and E_P. During brief intervals when VEFI's pre-amplifiers were subject to oscillations data outputs do not reflect geophysical conditions and are not plotted.

[5] The systematics of background E_{zonal} at low latitudes have been inferred from plasma flows detected by satellites [*Fejer et al.*, 2008] and from incoherent backscatter radar measurements [*Scherliess and Fejer*, 1997]. Vertical drifts caused by eastward electric fields ($E_{zonal} > 0$) are characterized by pre-reversal enhancements (PREs) near the dusk terminator. At post-sunset LTs plasma initially rises in response to polarization charges [*Farley et al.*, 1986]; and/or Sq current diversions [*Haerendel and Eccles*, 1992] near the terminator. After ~20:00 LT the direction of the vertical drift usually reverses, stabilizing the bottomside F-layer against irregularity growth. E_{zonal} normally remains westward across the nightside. Thus the PRE opens windows of opportunity for EPBs to form before damping dominates. PRE intensities have seasonal, longitudinal, and solar cycle dependencies, tending to be largest near solar-maximum equinoxes [*Scherliess and Fejer*, 1997]. At solar minimum PRE drifts are weak.

[6] Mechanisms responsible for post-midnight $E_{zonal} > 0$ at low latitudes include: (1) dusk-to-dawn, overshielding electric fields that appear in the recovery phases of storms

[1]Space Vehicles Directorate, Air Force Research Laboratory, Hanscom, AFB, Massachusetts, USA.
[2]NASA Goddard Space Flight Center, Greenbelt, Maryland, USA.

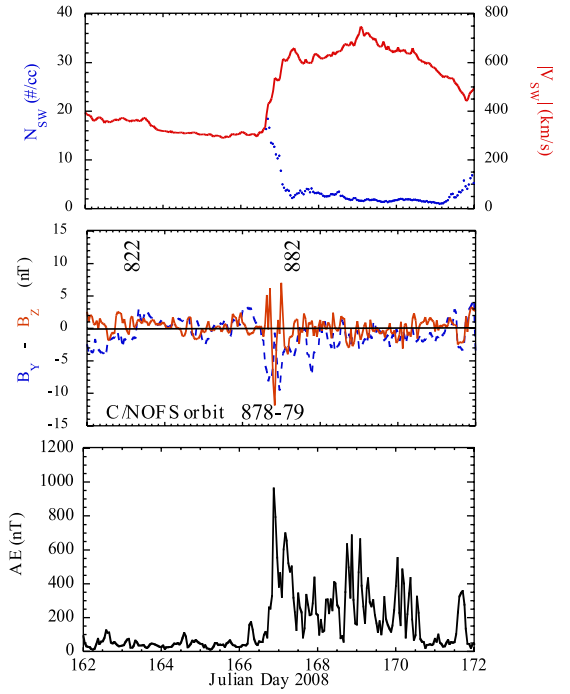

Figure 1. Interplanetary and auroral electrojet activity between 10 and 20 June 2008, including: solar wind densities (blue) and speeds (red) measured near (top) L_1, (middle) IMF B_Y (blue) and B_Z (red), and (bottom) the AE index.

and substorms [*Kikuchi et al.*, 2000, 2008] while Region 2 remain relatively strong, and (2) disturbance dynamos excited by Poynting and energetic particle fluxes into the auroral ionosphere [*Blanc and Richmond*, 1980; *Fejer and Scherliess*, 1995, 1997; *Scherliess and Fejer*, 1997]. *Blanc and Richmond* [1980] argued that heating at high latitudes drives equatorward winds. Associated equatorward Pedersen currents accumulate polarization charges at mid latitudes that drive plasma circulation in the anti-Sq sense with equatorial electric fields having eastward (westward) components on the nightside (dayside). *Fejer and Scherliess* [1995] demonstrated agreement between the LT distributions of radar measured vertical drifts and the model predictions. C/NOFS detections of post-midnight EPBs provide opportunities to weigh contributions of these mechanisms for producing $E_{zonal} > 0$ on the nightside. In principle, disturbance dynamo E_{zonal} produces relatively sustained increases in post-midnight EPB activity beginning a few hours after the disturbance onset and lasting up to 30 hours after they abate [*Scherliess and Fejer*, 1997]. Overshielding fields occur early in recovery while Region 2 currents relax at slower rates than those of Region 1 [*Kikuchi et al.*, 2000].

2. Observations

[7] Figure 1 summarizes interplanetary conditions observed by the Advanced Composition Explorer (ACE) satellite and induced geomagnetic responses during 10–20 June 2008 (Julian Days 162–172). The top plot shows solar wind densities N_{SW} (blue) and speeds V_{SW} (red) from measurements by the Solar Wind Electron Proton and Alpha Monitor [*McComas et al.*, 1998]. The second shows the interplanetary magnetic field (IMF), GSM B_Y (blue) and B_Z (orange) components measured by the Magnetic Field Instrument [*Smith et al.*, 1998]. The bottom plot is the AE index. While quantities in Figure 1 are hourly averages, our analyses use higher resolution data.

[8] On JD 166, V_{SW} rose from ~310 km/s at 16:00 UT to 640 km/s and remained >600 km/s though JD 170. N_{SW} data are unavailable prior to 15:36 UT on JD 166. As V_{SW} increased, N_{SW} first rose to 18.6 then fell to about 2 cm^{-3}. Combined N_{SW}-V_{SW} variations near 17:00 UT indicate that a corotating interaction region (CIR) formed at the leading edge of the HSS [*Balogh et al.*, 1999; *Tsurutani et al.*, 2006]. The IMF was weak both before V_{SW} increased and inside the HSS. Within the CIR transverse IMF components reached ~12 nT then rotated from northwest to south to northwest. From JD 162 to 166.5 AE was low 44.6 ± 24.3 nT with weak events excited by brief southward excursions. AE responded strongly to IMF turnings in the CIR and HSS. Peak excursions of 1311 and 1030 nT occurred at 21:27 UT on JD 166 and at 03:55 UT on JD 167, respectively. It remained high but erratic (237.0 ± 184.5 nT) as the HSS passed Earth.

[9] C/NOFS data are considered in two stages with N_i and E_{zonal} reported at 1-s cadences. Figure 2 shows N_i measurements from consecutive orbits near the CIR impact. Figure 3 contains N_i and E_{zonal} measurements representative nightside passes before and during the HSS passage. Unsurprisingly, N_i and E_{zonal} variations anti-correlate in regions of plasma irregularities. Before examining C/NOFS data it is useful to consider orbital constraints that influence interpretations. On 10 June C/NOFS' perigee and ascending node were near 01:00 and 19:00 LT. The ascending node's longitude progresses ~24.2° to the west on successive orbits. C/NOFS thus provides 3 to 4 snapshots of the nightside ionosphere at a given longitude, albeit at different latitudes and altitudes. Orbital lines of apsides and nodes precessed ~7.5° to the east and ~8.25° to the west per day, respectively. C/NOFS approached perigee after local midnight. Locations of the ascending node and perigee placed C/NOFS north of the geographic equator at nightside LTs. Perigee was near the magnetic equator in the African to central Pacific sector but at Appleton anomaly magnetic latitudes at eastern Pacific to South American longitudes.

[10] Figure 2 shows N_i measurements from late on 14 June. Double arrows mark the durations of C/NOFS orbits 878 and 879. The letters M and P mark midnight and perigee crossings. Horizontal bars span periods when

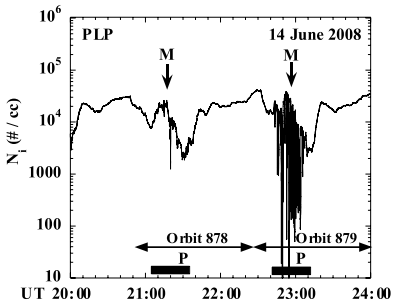

Figure 2. PLP plasma densities measured between 20:00 and 24:00 UT on 14 June 2008. Times of C/NOFS orbits 878 and 879 are indicated along with midnight meridian (M) and perigee (P) crossings. Solid bars mark intervals when C/NOFS was in darkness.

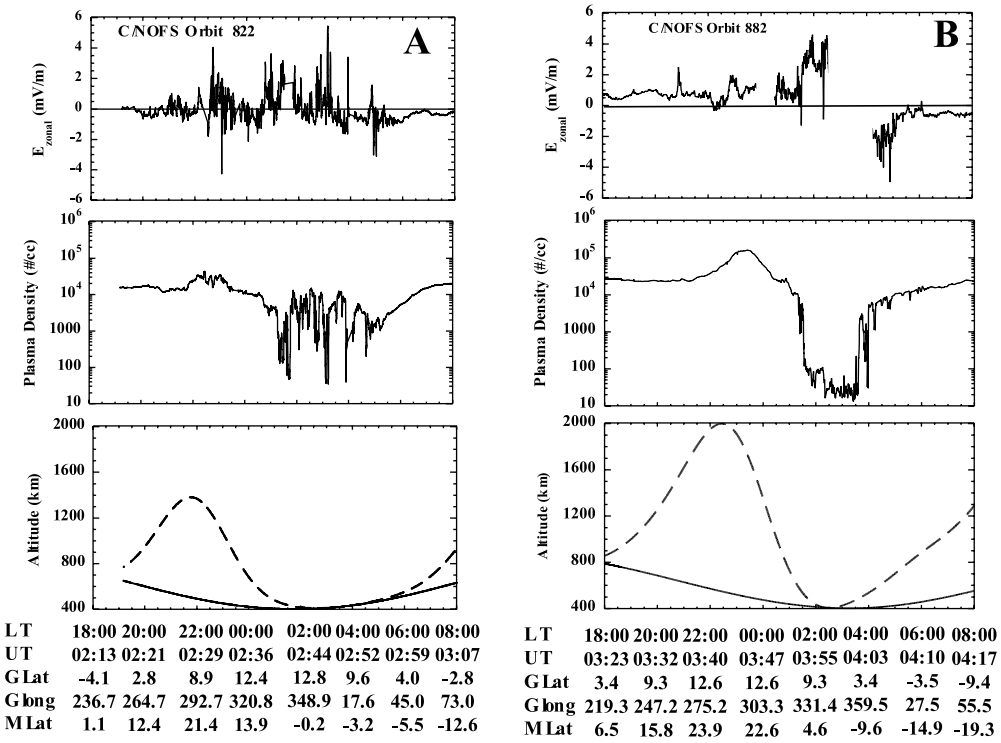

Figure 3. (top) Zonal electric fields and (middle) plasma densities measured by C/NOFS during orbits (a) 822 and (b) 882, plotted as functions of LT, UT, geographic latitude, geographic longitude, and geomagnetic latitude. Orbit 822 illustrates predisturbance conditions; orbit 882 occurred shortly after the CIR passage. (bottom) Traces indicate geographic altitudes (solid lines) of C/NOFS and the apex altitudes of magnetic field lines on which measurements were made.

C/NOFS was in darkness. During the eclipsed portions of orbits 878 and 879 C/NOFS crossed longitudes $-10°$ to 105°E and $-35°$ to 80°E, respectively. Thus, both passes covered African to Indian Ocean longitudes. Except for one depletion near 21:20 UT (00:45 LT, ~50°E) δN_i amplitudes were small during orbit 878. Conversely, on orbit 879 C/NOFS encountered continuous large $\delta N_i/N_i >$ 100 irregularities from eastern Atlantic through African longitudes. Pre-midnight EPBs apparent on orbit 879 are singular exceptions to the post-midnight rule for these ten days. Expanded views of N_i (not given) indicate that local δN_i depressions were 110 to 480 km wide. The African sector is common to both observations. Thus, differences observed between orbit 878 and 879 are time dependent. Note that the first AE peak occurred ~1 hour before the start of orbit 879.

[11] Figure 3 shows E_{zonal} (Figure 3, top) and N_i (Figure 3, middle) sampled at similar longitudes during C/NOFS orbits 822 (Figure 3a) and 882 (Figure 3b). These data were acquired during the magnetically quiet/disturbed JD 163/167, respectively and are plotted as functions of LT beginning at ascending nodes, UT, geographic latitude (GLat), geographic longitude (GLong) and corrected magnetic latitude (MLat). The bottom plots indicate spacecraft altitudes (solid lines) and apex altitudes of magnetic field lines (dashed lines). Traces converge where C/NOFS was near the magnetic equator.

[12] Plasma densities shown in Figure 3a increased at pre-midnight LTs as the C/NOFS altitude decreased. Evening sector irregularities appear as weak local increases and decreases. Starting at ~23:00 LT while C/NOFS was descending, N_i decreased gradually. After local midnight N_i fell precipitously near perigee. From ~01:00 LT through dawn C/NOFS crossed a series of (factors of 10 to 100) EPB depletions; E_{zonal} was irregular and eastward within the depletions. C/NOFS remained close to the magnetic equator as its trajectory rose from perigee. Figure 3b (middle) shows a pre-midnight N_i enhancement followed by post-midnight irregularities and depletions, but EPB signatures were infrequent. Rather, C/NOFS crossed a wide (~3500 km) plasma density trench from ~03:53 to 04:01 UT (01:45-04:00 LT) on JD 167. Across this deep depletion, the average E_{zonal} was ~2.4 mV/m eastward (Figure 3b, top). After 03:56:15 UT, (~02:30 LT) when the plasma density abruptly fell to ~20 cm^{-3}, E_{zonal} variations increased dramatically but with no correspondence to simultaneous changes in measured δNi. At these low densities the Debye length grew to ~1 m. Thus, observed E_{zonal} fluctuations probably reflect responses to differences in VEFI's sheath impedances. We note, but do not show, that the large-amplitude irregularities of orbit 879 appear to have evolved into the broad trench. During nightside parts of orbits 880 and 881, C/NOFS encounters with topside plasma diminished and the longitudinal scale sizes of N_i depletions widened. The deep depletion of orbit 882 narrowed during orbit 883 then disappeared as the affected ionosphere rotated into the dayside.

[13] Data acquired during nightside passes of Figure 3 also illustrate relationships between N_i (blue) and E_{zonal} (red). During orbit 822 δN_i and δE_{zonal} strongly anti-correlated, E_{zonal} intensified within N_i depletions. This is consistent with C/NOFS' passing through upwelling EPBs permeated by

strong polarization electric fields [*Ott*, 1978]. This relationship continued during orbit 882, from 03:54–03:55 UT, while C/NOFS was in the western part of the deep plasma trench. However, at ~03:56:13 UT as N_i rapidly decreased from to ~15 cm^{-3}, δE_{zonal} underwent large amplitude oscillations related to large sheaths around VEFI. The quasi DC portion of E_{zonal} was ~2.4 mV/m across the orbit 882 plasma trench, consistent with the local F layer being lifted above C/NOFS.

3. Discussion

[14] This study focused on dynamics of the nightside, equatorial ionosphere before and during passage of a HSS in the solar wind. During this period C/NOFS' perigee was at post-midnight LTs. Interplanetary and AE data show three distinct intervals, (1) geomagnetic quiet, JD 162–166.5, (2) responses to the CIR magnetic field rotation JD 166.5–167, and (3) HSS induced activity JD 167–170.

[15] Figure 3a (middle) shows that from the western Atlantic across Africa to the central Pacific (~160°E) C/NOFS detected pre-disturbance EPBs and large depletions after midnight. At other longitudes C/NOFS was away from the magnetic equator. Even during sustained periods of magnetic quiet in solar minimum bottomside irregularities grew into EPBs. This raises a question. What mechanism supports the development of EPBs at post-midnight LTs during quiet intervals when neither overshielding nor disturbance dynamo E_{zonal} fields can operate? Solar UV fluxes driving dayside dynamos and consequent PRE signatures were also weak. With no post-dusk westward E_{zonal} to stabilize the bottomside ionosphere, the gravitational drift current $j_G = n_i(m_i\mathbf{g} \times \mathbf{B})/B^2$ has no competitors. Normally insufficient time is available for j_G to drive bottomside irregularities into the nonlinear regime before E_{zonal} turns westward [*Basu*, 1997]. If $E_{zonal} \approx 0$, data suggest that enough time becomes available for EPBs to grow and reach altitudes ≥400 km after midnight.

[16] Figure 2 shows that the nightside ionosphere responded to the CIR passage. Except for the high number of EPBs encountered during orbit 879 the upper envelopes of N_i traces for orbits 878 and 879 were similar. The R-T growth rate equation [*Ott*, 1978] suggests that an eastward E_{zonal} was present on the nightside during the hour before C/NOFS orbit 879. AE first peaked at 21:27 UT then decreased at a rate of 283 nT/hr. *Scherliess and Fejer* [1997] estimated that several hours are needed for disturbance-dynamo effects to reach the equator. On the other hand, overshielding electric fields appear soon after the IMF turns northward [*Kikuchi et al.*, 2000]. We suggest that overshielding was primarily responsible for changes seen between orbits 878 and 879.

[17] During orbit 882 C/NOFS crossed a broad and deep depletion with average $E_{zonal} \approx 2.4$ mV/m. With an equatorial magnetic field of ~31,000 nT, this corresponds to upward drifts of ~77 m/s. It would take ~22 minutes for the F layer to rise 100 km. Thus, within this deep trench C/NOFS sampled plasma that originated far below the peak height of the quiescent F layer. Between JD 167 and 170 C/NOFS witnessed several cycles of plasma and AE quieting and activation. With available information it is difficult to distinguish between overshielding and disturbance-dynamo contributions. However, the average $E_{zonal} \approx 2.4$ mV/m measured across the deep plasma trench seems to be a disturbance dynamo effect. Early on JD 167 the downward trend of AE reversed, reaching a second peak of 1030 nT at 03:55 UT. It appears unlikely that an overshielding E_{zonal} operated in the hour prior to orbit 882. Within the bounds of present understanding only the disturbance dynamo can explain the strong eastward E_{zonal} measured during orbit 882.

4. Conclusions

[18] This study of C/NOFS measurements indicates that during June 2008 EPBs and deep plasma trenches formed at post-midnight LTs. These features were present during an extended period of magnetic quiet, but intensified after the CIR's coupling to the magnetosphere-ionosphere weakened and allowed the auroral electrojet to relax. Observed EPB activity waxed and waned as the HSS passed Earth. Our analysis supports four conclusions:

[19] 1. Active post-midnight EPBs carry eastward polarization electric fields and indicate that irregularities can form and reach C/NOFS altitudes even during magnetically quiet intervals in solar minimum. Under these conditions $n_i m_i(\mathbf{g} \times \mathbf{B})$ currents acquire sufficient time to drive nonlinear R-T instabilities.

[20] 2. Intensification of EPB activity, observed about an hour after the CIR-induced peak in AE, was probably caused by eastward overshielding electric fields.

[21] 3. The plasma trench of orbit 882 with $E_{zonal} \approx 2.4$ mV/m was observed while AE was increasing and thus appears to be mostly a disturbance dynamo effect.

[22] 4. Continued, albeit sporadic, detections of EPBs and plasma trenches during the four days of the HSS passage suggest that both overshielding and disturbance dynamos remained active. Presently available information is insufficient to distinguish their distinctive contributions.

[23] **Acknowledgments.** The C/NOFS mission is supported by the Air Force Research Laboratory, the Department of Defense Space Test Program, the National Aeronautics and Space Administration, the Naval Research Laboratory, and the Aerospace Corporation. This analysis was supported by Air Force Office of Scientific Research Task 2301SDA5 and Air Force contract FA8718-08-C-0012 with Boston College.

References

Balogh, A., J. T. Gosling, J. R. Jokipii, R. Kallenbach, and H. Kunow (Eds.) (1999), Corotating interaction regions, *Space Sci. Rev.*, *89*, 141, doi:10.1023/A:1005245306874.

Balsley, B. B., G. Haerendel, and R. A. Greenwald (1972), Equatorial spread F: Recent observations and a new interpretation, *J. Geophys. Res.*, *77*, 5625, doi:10.1029/JA077i028p05625.

Basu, B. (1997), Generalized Rayleigh-Taylor instability in the presence of time-dependent equilibrium, *J. Geophys. Res.*, *102*, 17,305, doi:10.1029/97JA01239.

Blanc, M., and A. D. Richmond (1980), The ionospheric disturbance dynamo, *J. Geophys. Res.*, *85*, 1669, doi:10.1029/JA085iA04p01669.

Burke, W. J. (1979), Plasma bubbles near the dawn terminator in the topside ionosphere, *Planet. Space Sci.*, *27*, 1187, doi:10.1016/0032-0633(79)90138-7.

de La Beaujardière, O., and C/NOFS Science Definition Team (2003), Communication/Navigation Outage Forecasting System (C/NOFS) science plan, *Rep. AFRL/VS-TR-2003-1501*, Air Force Res. Lab., Hanscom AFB, Mass.

Eccles, J. V. (2004), The effect of gravity and pressure in the electrodynamics of the low-latitude ionosphere, *J. Geophys. Res.*, *109*, A05304, doi:10.1029/2003JA010023.

Farley, D., E. Bonelli, B. Fejer, and M. Larsen (1986), The prereversal enhancement of the zonal electric field in the equatorial ionosphere, *J. Geophys. Res.*, *91*, 13,723, doi:10.1029/JA091iA12p13723.

Fejer, B. G., and L. Scherliess (1995), Time dependent response of equatorial ionospheric electric fields to magnetospheric disturbances, *Geophys. Res. Lett.*, *22*, 851, doi:10.1029/95GL00390.

Fejer, B. G., and L. Scherliess (1997), Empirical models of storm time equatorial zonal electric fields, *J. Geophys. Res.*, *102*, 24,047, doi:10.1029/97JA02164.

Fejer, B. G., J. W. Jensen, and S.-Y. Su (2008), Quiet time equatorial F region plasma drift model derived from ROCSAT observations, *J. Geophys. Res.*, *113*, A05304, doi:10.1029/2007JA012801.

Greenspan, M. E., C. E. Rasmussen, W. J. Burke, and M. A. Abdu (1991), Equatorial density depletions observed at 840 km during the great magnetic storm of March 1989, *J. Geophys. Res.*, *96*, 13,931, doi:10.1029/91JA01264.

Haerendel, G., and J. V. Eccles (1992), The role of the equatorial electrojet in the evening ionosphere, *J. Geophys. Res.*, *97*, 1181, doi:10.1029/91JA02227.

Kikuchi, T., H. Lühr, K. Schlegel, H. Tachihara, and T.-I. Kitamura (2000), Penetration of auroral electric fields to the equator during a substorm, *J. Geophys. Res.*, *105*, 23,251, doi:10.1029/2000JA900016.

Kikuchi, T., K. K. Hashimoto, and K. Nozaki (2008), Penetration of magnetospheric electric fields to the equator during geomagnetic storms, *J. Geophys. Res.*, *113*, A06214, doi:10.1029/2007JA012628.

McComas, D. J., S. J. Bame, P. Barber, W. C. Fieldman, J. L. Phillips, and P. Riley (1998), Solar wind electron, proton, and alpha monitor (SWEPAM) on the Advanced Composition Explorer, *Space Sci. Rev.*, *86*, 563, doi:10.1023/A:1005040232597.

Ott, E. (1978), Rayleigh-Taylor bubbles in the equatorial ionosphere, *J. Geophys. Res.*, *83*, 2066, doi:10.1029/JA083iA05p02066.

Scherliess, L., and B. G. Fejer (1997), Storm time dependence of equatorial disturbance dynamo zonal electric fields, *J. Geophys. Res.*, *102*, 24,037, doi:10.1029/97JA02165.

Smith, C. W., M. H. Acuña, L. F. Burlaga, J. L. L'Heureux, N. F. Ness, and J. Scheifele (1998), The ACE magnetic field experiment, *Space Sci. Rev.*, *86*, 613, doi:10.1023/A:1005092216668.

Tsurutani, B. T., et al. (2006), Corotating solar wind streams and recurrent geomagnetic activity: A review, *J. Geophys. Res.*, *111*, A07S01, doi:10.1029/2005JA011273.

W. J. Burke, O. de La Beaujardière, L. C. Gentile, D. E. Hunton, P. A. Roddy, Y.-J. Su, and G. R. Wilson, Space Vehicles Directorate, Air Force Research Laboratory, 29 Randolph Road, Hanscom AFB, MA 01731-3010, USA. (afrl.rvb.pa@hanscom.af.mil)

R. F. Pfaff, NASA Goddard Space Flight Center, Mail Code 674, Greenbelt, MD 20771, USA.

Assimilative modeling of equatorial plasma depletions observed by C/NOFS

Y.-J. Su,[1] J. M. Retterer,[1] O. de La Beaujardière,[1] W. J. Burke,[1,2] P. A. Roddy,[1] R. F. Pfaff Jr.,[3] G. R. Wilson,[1] and D. E. Hunton[1]

Received 29 April 2009; revised 2 June 2009; accepted 9 June 2009; published 22 July 2009.

[1] Using electric field measurements as inputs, the assimilative physics-based ionospheric model (PBMOD) successfully reproduced density depletions observed at early morning local times during four consecutive orbits of the Communication/Navigation Outage Forecasting System (C/NOFS) satellite on 17 June 2008. However, the PBMOD running with plasma drift data from empirical models as inputs predicted neither plasma depletions nor irregularities on this day. Coincident over flights of a large depletion by C/NOFS and the DMSP-F17 satellite allow estimates of its longitudinal and latitudinal scale sizes. The satellite-based estimates are shown to be in reasonable agreement with PBMOD predictions. The model's reproduction of observed temporal and spatial distributions of plasma depletions suggests that our assimilative technique can be used to enhance space-weather forecasts. **Citation:** Su, Y.-J., J. M. Retterer, O. de La Beaujardière, W. J. Burke, P. A. Roddy, R. F. Pfaff Jr., G. R. Wilson, and D. E. Hunton (2009), Assimilative modeling of equatorial plasma depletions observed by C/NOFS, *Geophys. Res. Lett.*, *36*, L00C02, doi:10.1029/2009GL038946.

1. Introduction

[2] Properties of low-latitude plasma irregularities, commonly observed at post-sunset local times, have been studied extensively using ground and satellite-based measurements [e.g., *Fejer and Kelley*, 1980; *Fejer*, 1997]. The pre-reversal enhancement of upward plasma drifts, due to eastward polarization electric fields, is the primary cause of these irregularities [e.g., *Richmond*, 1995]. On the other hand, reported plasma depletions at post-midnight and early morning local times are scarce. The majority of reported events occurred during storm time conditions [e.g., *Burke*, 1979; *Su et al.*, 2004]. In a rare occurrence during solar maximum, ROCSAT-1 simultaneously observed an intense reduction in ion density with super-cool temperatures, accompanied by large downward, eastward, and field-aligned flows near the dawn meridian [*Su et al.*, 2004]. *Burke* [1979] suggested that dawn bubbles may be caused by substorm-generated eastward electric fields at the equator or by travelling ionospheric disturbances. In a theoretical/numerical study, *Eccles* [2004] showed a persistent 10 m s^{-1} pre-sunrise uplift of the ionosphere due to gravity-driven current. In a statistical study by *Sobral et al.* [1999], two cases were found between 1980 and 1992 in the post-midnight sector during quiet times in which plasma depletions were observed. C/NOFS frequently encounters deep plasma depletions at the dawn terminator, particularly in June and September 2008. We have analyzed density and electric field irregularities at post-midnight local times during a 10-day period in June 2008 during which a fast stream in the solar wind passed the Advanced Composition Explorer (ACE) satellite. This paper describes equatorial ionospheric responses observed in the early morning local times on 17 June 2008 while a solar wind fast stream was passing Earth for comparison with predictions of the physics-based ionospheric model (PBMOD) [*Retterer*, 2005; *Retterer et al.*, 2005]. PBMOD operates in both assimilative and climatological modes. The former mode is done with electric field measurements from the Vector Electric Field Instrument (VEFI) on C/NOFS. The latter has no electric-field information beyond that provided by climatological models [e.g., *Scherliess and Fejer*, 1999]. Plasma densities obtained from both types of simulation are compared with measurements by the Planar Langmuir Probe (PLP) on C/NOFS.

2. Model Description

[3] The simulation tool used in this study was developed by *Retterer* [2005] over the last decade at the Air Force Research Laboratory to support the C/NOFS mission analysis. This 4-D model of the low-latitude ionosphere solves the continuity equation as functions of position and time along magnetic field lines over a range of apex altitudes. The climatological version of the simulation is carried out with initial conditions such as neutral winds and temperatures, ion production and loss rates, and plasma density and temperature prescribed by various empirical models [*Retterer et al.*, 2005]. The assimilative version input data consist of available satellite and/or ground measurements as inputs. In this study, the only ingested data are $\boldsymbol{E} \times \boldsymbol{B}$ drift velocities calculated from VEFI electric field measurements and the International Geomagnetic Reference Field (IGRF) model [*Maus et al.*, 2005]. We note that the VEFI instrument also provides magnetic field measurements. The magnetic field strength obtained from IGRF is within 1% of the measured value. Whenever electric field data were unavailable, such as simulation regions far away from the spacecraft trajectory, we used climatological values from an empirical drift model based on Jicamarca radar and the Atmospheric Explorer satellite data [*Scherliess and Fejer*, 1999]. *Retterer* [2005] provides a fuller description of the assimilative procedures.

[1] Space Vehicles Directorate, Air Force Research Laboratory, Hanscom Air Force Base, Bedford, Massachusetts, USA.
[2] Institute for Scientific Research, Boston College, Chestnut Hill, Massachusetts, USA.
[3] NASA Goddard Space Flight Center, Greenbelt, Maryland, USA.

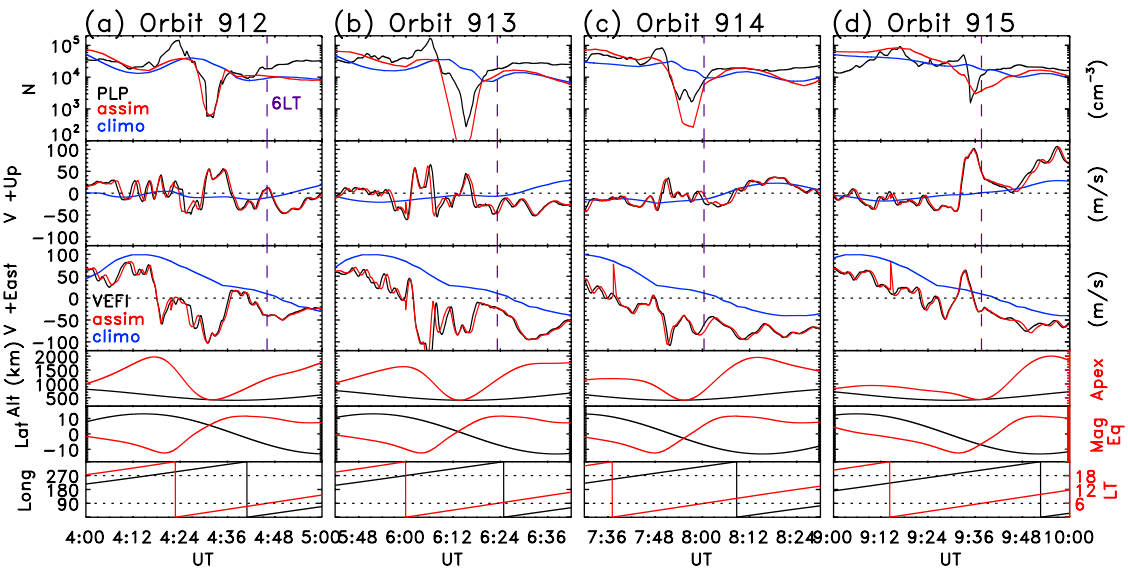

Figure 1. Four one-hour segments of data at (a) 04:00–05:00, (b) 05:42–06:42, (c) 07:30–08:30, and (d) 09:00–10:00 UT. From top to bottom plots: ion densities, vertical and zonal drift velocities, and satellite altitude, latitude, and longitude.

[4] Although PBMOD was designed as a tool to study both coarse-scale global ionospheric structures and fine-scale localized plasma turbulences, this paper focuses only on large-scale density depletions observed at post-midnight local times on 17 June 2008 (day of year 169). While the average *Kp* index was ∼2 on this solar-minimum day, the auroral electroject (*AE*) index showed large amplitude variations typical of fast stream intervals [*Tsurutani and Gonzalez*, 1987]. The simulated low-latitude ionosphere is divided into 36 longitudinal sectors of 10° width. The latitudinal grid has 201 steps along each field line. The vertical grid has 60 points varying in size and ranges for field-line apex altitudes between 140 and 4000 km. The simulation time step is 6 min. Throughout this report simulation results and satellite observations are presented in geographic coordinates.

3. Results

[5] Although PBMOD was run in both the assimilative and climatological modes for the entire day of 17 June 2008, here we focus on four one-hour segments that include consecutive C/NOFS nightside passes labeled 912–915 in Figures 1a–1d. Black, blue, and red lines in Figures 1a–1d represent C/NOFS observations, climatology results, and assimilative model outputs, respectively. Ion densities are plotted followed by the vertical and zonal drift velocities; positive values indicate upward and eastward drifts. Before assimilating electric fields into the global model, we applied a low-pass Fourier filter [*Retterer*, 2005] with a 5-min window to 1-second averaged VEFI and PLP data to remove small-scale variations (represented by the black lines in top three plots of Figure 1). The vertical dashed lines in the top three plots of Figure 1 mark times when C/NOFS crossed the 06:00 LT meridian. The C/NOFS altitude and the apex altitude of the field line it occupies are represented by black and red lines in the fourth plot from the top. The satellite latitude and the magnetic equator are plotted as black and red lines in the fifth panel. Intersections of the red and black lines in plots 4 and 5 of Figure 1 mark satellite crossings of the magnetic equator. Black and red lines in Figure 1 (bottom) indicate the longitudes and local times of the spacecraft; the horizontal dotted lines denote 06:00 and 18:00 LT.

[6] As seen in Figure 1 (top) large-scale density depletions were observed during four consecutive satellite orbits when eastward electric fields (e.g., upward velocities) were observed by VEFI (black lines in the second plot of Figure 1) when or a few minutes before the satellite encountered the depletion. C/NOFS crossed all of the depletions presented here at early morning local times while flying at or near the magnetic equator. PBMOD reproduced the main qualitative features of the pre-dawn sector depletions (red lines) observed by PLP (black lines) based on assimilations of available electric field data obtained from VEFI (red lines in the 2nd and 3rd plots of Figure 1). Conversely, no plasma depletions or irregularities were predicted while exercising the climatological version (blue lines) with input drift velocities derived from empirical models.

[7] It is impossible to specify both the latitude and longitude scale sizes of plasma depletions with measurements from a single satellite. Fortunately, the F17 satellite of the Defense Meteorological Satellite Program (DMSP) crossed the same depletion structure at a higher altitude (860 km) ∼10 min prior to the C/NOFS encounter at 420 km (cf. Figure 1d). The tracks of the two satellite orbits are illustrated in Figure 2b. DMSP-F17 crossed the depletion moving north to south at 09:12–09:36 UT, while C/NOFS traversed it moving west to east at 09:24–09:48 UT. Corresponding density measurements at 1 sec resolution from DMSP and C/NOFS are plotted in Figures 2a and 2c, respectively. Note that the time scale increases downward in Figure 2a. The dotted lines in Figures 2a and 2c mark our estimates of the depletion boundaries. If we assume that the plasma density structure did not change significantly during the 10 min time offset, the dimensions of the depletion are about 14° in longitude and 21° in latitude, corresponding to the heavy-line segments of the trajectories in Figure 2b.

[8] A comparison of simulation results with the two satellite observations is presented in Figure 3. It shows O^+ density outputs from PBMOD calculated using assimilated VEFI (Figure 3a) and climatological values for the velocity drifts (Figure 3b). Recall that each time step of PBMOD simulations is 6 min. As indicated above Figure 3, the 2D plots represent conditions at 09:36 UT and 4°S. Red stars indicate C/NOFS' location at 9:35 UT when it sampled the density minimum (295°E, 5°S); black stars mark DMSP-F17's location at 09:25UT (300°E, 5°S). Climatology-based model results, shown in Figure 3b, indicate low nightside densities in the bottom-side ionosphere. Just prior to sunrise the predicted altitude of the peak of the F_2 layer (h_mF_2) is at ~300 km. By contrast, assimilation-based results displayed in Figure 3a indicate that the ionosphere was lifted upward. Near times when the two satellites encountered the deep depletion h_mF_2 had reached ~900 km altitude. DMSP-F17 was flying below the F_2 peak. The longitudinal extent of the depletion is ~30°. In order to demonstrate the predicted latitudinal dimension of the depletion, Figure 3c shows assimilation (red) and climatological (black) predictions of peak F-layer densities (N_mF_2) plotted as functions of latitude at 09:36 UT and 285°E. The climatologically predicted latitudinal separation between the two N_mF_2 maxima (the equatorial ionospheric anomaly) was 18°. The latitudinal width of density valley increased to 32° in assimilation-model calculations. The size of the density depletion estimated from the two satellites shown in Figure 2 is within the dimension of the depletion structure derived from the assimilative simulation results shown in Figures 3a and 3c.

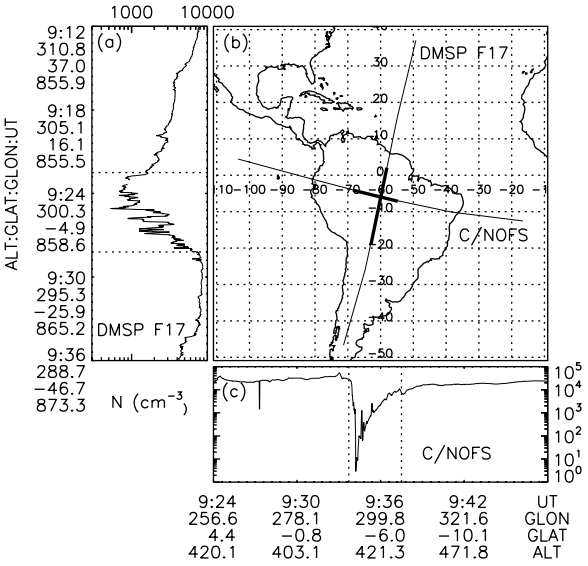

Figure 2. (a) Total ion densities measured by SSIES on board DMSP-F17 from 9:12 to 9:36 UT, where the y-axis label include UT, longitude, latitude, and altitude information of the satellite. (b) DMSP-F17 crossed the equator from north to south, while C/NOFS traversed South America from west to east 10 *min* after the DMSP pass. (c) The ion densities observed by PLP on board C/NOFS from 9:24 to 9:48 UT. The boldfaced cross in Figure 2b indicates an estimated depletion region corresponding to the dotted lines in Figures 2a and 2c.

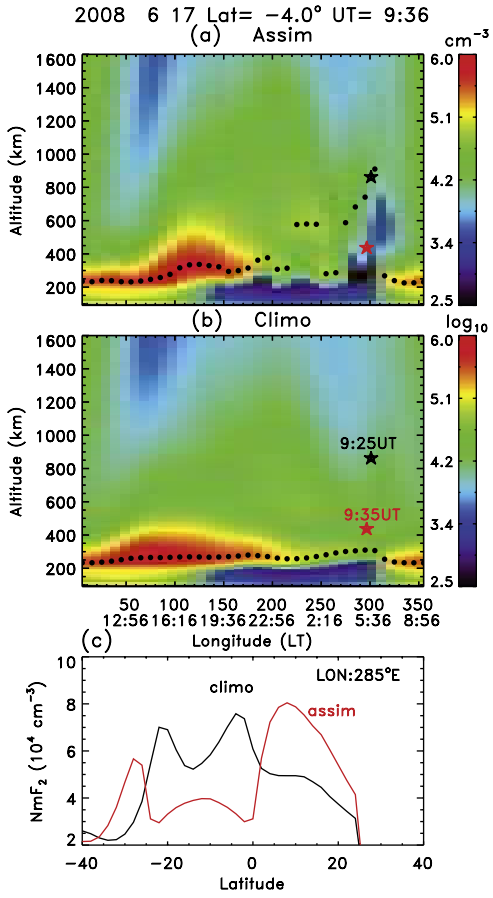

Figure 3. (a) 2D density map obtained from the assimilation model, where the x- and y- axis represent longitude and altitude, respectively. (b) 2D density map based on the climatology model output. The black and red star symbols in Figures 3a and 3b denote the DMSP-F17 and C/NOFS satellite locations when the minimum densities were observed at 9:25 and 9:35 UT, respectively. The black dots indicate local *hmF2*. (c) 1D plot of N_mF_2 as a function of geographical latitude, where the red and black lines represent results from the assimilation and climatology models, respectively.

[9] An examination of the temporal evolution of density maps derived from PBMOD (see Animation S1 of the auxiliary material) indicates that the density depletions shown in Figures 1a–1d should be regarded as passing through the same structure during four consecutive C/NOFS orbits.[1] This structure expands or shrinks in response to the history of vertical plasma drifts (zonal electric fields). Figure 3a shows that, at longitudes > 310°E, the bottom-side of the *F*-layer began to refill with plasmas created after sunrise, while topside densities remained low. Several minutes later, the bottom-side density depletion (<400 km between 280°E and 310°E longitude) extended further into normally topside altitudes due to large upward velocities observed at 09:36 UT (second plot of Figure 1d). However,

[1]Auxiliary materials are available in the HTML. doi:10.1029/2009GL038946.

the longitudinal width of the depletion continued to decrease with time as its most eastward portion crossed the dawn terminator where the ionosphere was replenished with new plasmas generated by photoionization.

4. Summary and Discussion

[10] The assimilative version of PBMOD that had VEFI inputs reproduced qualitative large-scale features of density depletions observed near dawn by the PLP during four consecutive C/NOFS orbits on 17 June 2008. No plasma depletions or irregularities were predicted by the climatology version of the model. DMSP-F17 and C/NOFS made north-to-south and west-to-east cuts through the same density depletion structure within 10 min of each other. At the times of these encounters the latitudinal and longitudinal dimensions of the depletion are $\sim$21° and 14°, respectively. This observational result is within the estimated 32° by 30° size of the density depletion derived from assimilative modeling results. Consistent with observations of the depletion at 420 and 860 km, the assimilation indicated that h_mF_2 reached altitudes near 900 km.

[11] A significant advantage of the 4D physics-based modeling is to provide reasonable global information of ionospheric responses when and where *in-situ* satellite observations are not available. Assimilative modeling results confirm that C/NOFS sampled the same density depletion in four orbits between 04:00 and 10:00 UT. As the depletion crossed the dawn terminator it began to refill with fresh plasmas from the lower ionosphere. The depletion structure expanded and contracted in response to the history of zonal electric fields. The uplift of the ionosphere is due to an eastward electric field, while westward electric fields act to stabilize the nightside ionosphere. The cause of the large-scale dawn density depletion is similar to that of post-sunset plasma irregularities or bubbles, however, their generation mechanisms are different.

[12] Plasma density depletions discussed in this paper were observed during solar minimum when the average $F_{10.7}$ was $\sim$67. The gravity-driven current suggested by *Eccles* [2004] may be the dominant effect to explain the dawn depletion during extended quiet geomagnetic conditions. Upward drifts of 10–15 m s^{-1} at dawn due to $m_i\boldsymbol{g} \times \boldsymbol{B}$ currents, as estimated by *Eccles* [2004], are considerably smaller than those inferred from VEFI measurements on 17 June 2008. We cannot rule out contributions from disturbance dynamos [*Scherliess and Fejer*, 1997] excited after a corotating interaction region (CIR) at the leading edge of a fast solar wind stream observed by ACE at $\sim$16 UT on 14 June. Large excursions of the *AE* index occurred at 21 UT on 16 June and at 2 UT on 17 June. Overshielding eastward fields may be induced when Region 2 currents exceed those of Region 1 when *AE* decreases rapidly [*Kikuchi et al.*, 2000]. Further investigation is needed in order to separate various contributions in the generation of eastward electric fields.

[13] Small-scale variations in the drift velocities have been smoothed by a low-pass filter prior to use as input for the global run of PBMOD in order to maintain a reasonable model run-time for forecasting purpose. As a result, this study is limited in scope to an examination of large density structures in the ambient ionosphere. The spatial and temporal resolution of the global PBMOD run can be enhanced with increased computing power. The small-scale density irregularities, such as equatorial bubbles or spread *F*, can be further investigated by the regional plume model algorithms in PBMOD [*Retterer*, 2005].

[14] The neutral wind plays an important role in the thermosphere-ionosphere dynamics. In future studies, we plan to incorporate measurements obtained from the Neutral Wind Meter on C/NOFS for PBMOD assimilation to investigate the neutral wind effect and to further validate the space weather forecasting capabilities.

[15] **Acknowledgments.** The C/NOFS mission is supported by the Air Force Research Laboratory, the Department of Defense Space Test Program, the National Aeronautics and Space Administration, the Naval Research Laboratory, and the Aerospace Corporation. The analysis was supported in part by Air Force Office of Scientific Research Task 2301SDA5, Air Force contract FA8718-08-C-0012 with Boston College, and NASA grant NNH09AK05I to the Air Force Research Laboratory.

References

Burke, W. J. (1979), Plasma bubbles near the dawn terminator in the topside ionosphere, *Planet. Space Sci.*, *27*, 1187, doi:10.1016/0032-0633(79)90138-7.

Eccles, J. V. (2004), The effect of gravity and pressure in the electrodynamics of the low-latitude ionosphere, *J. Geophys. Res.*, *109*, A05304, doi:10.1029/2003JA010023.

Fejer, B. G. (1997), The electrodynamics of the low-latitude ionosphere: Recent results and future challenges, *J. Atmos. Sol. Terr. Phys.*, *59*, 1465, doi:10.1016/S1364-6826(96)00149-6.

Fejer, B. G., and M. C. Kelley (1980), Ionospheric irregularities, *Rev. Geophys.*, *18*, 401, doi:10.1029/RG018i002p00401.

Kikuchi, T., H. Liihr, K. Schlegel, H. Tachihara, M. Shinohara, and T.-I. Kitamura (2000), Penetration of auroral electric fields to the equator during a substorm, *J. Geophys. Res.*, *105*, 23,251, doi:10.1029/2000JA900016.

Maus, S., S. MacMillan, F. Lowes, and T. Bondar (2005), Evaluation of candidate geomagnetic field models for the 10th generation of IGRF, *Earth Planets Space*, *57*, 1173.

Retterer, J. M. (2005), Physics-based forecasts of equatorial radio scintillation for the Communication and Navigation Outage Forecasting System (C/NOFS), *Space Weather*, *3*, S12C03, doi:10.1029/2005SW000146.

Retterer, J. M., D. T. Decker, W. S. Borer, R. E. Daniell Jr., and B. G. Fejer (2005), Assimilative modeling of the equatorial ionosphere for scintillation forecasting: Modeling with vertical drifts, *J. Geophys. Res.*, *110*, A11307, doi:10.1029/2002JA009613.

Richmond, A. D. (1995), Modeling equatorial ionospheric electric fields, *J. Atmos. Terr. Phys.*, *57*, 1103, doi:10.1016/0021-9169(94)00126-9.

Scherliess, L., and B. G. Fejer (1997), Storm time dependence of equatorial disturbance dynamo zonal electric fields, *J. Geophys. Res.*, *102*, 24,037, doi:10.1029/97JA02165.

Scherliess, L., and B. G. Fejer (1999), Radar and satellite global equatorial *F* region vertical drift model, *J. Geophys. Res.*, *104*, 6829, doi:10.1029/1999JA900025.

Sobral, J. H. A., M. A. Abdu, H. Takahashi, H. Sawant, C. J. Zamlutti, and G. L. Borba (1999), Solar and geomagnetic activity effects on nocturnal zonal velocities of ionospheric plasma depletions, *Adv. Space Res.*, *24*, 1507, doi:10.1016/S0273-1177(99)00716-4.

Su, S.-Y., H. C. Yeh, C. K. Chao, and R. A. Heelis (2004), Supercooled ion temperatures observed in the topside ionosphere at dawn meridian during storm periods, *J. Geophys. Res.*, *109*, A06307, doi:10.1029/2003JA010139.

Tsurutani, B. T., and W. D. Gonzalez (1987), The cause of high intensity long-duration continuous AE activity (HILDCAAs): Interplanetary Alfvén wave trains, *Planet. Space Sci.*, *35*, 405, doi:10.1016/0032-0633(87)90097-3.

O. de La Beaujardière, W. J. Burke, D. E. Hunton, J. M. Retterer, P. A. Roddy, Y.-J. Su, and G. R. Wilson, Air Force Research Laboratory, 29 Randolph Road, Hanscom AFB, MA 01731, USA. (yi-jiun.su@hanscom.af.mil)

R. F. Pfaff Jr., NASA Goddard Space Flight Center, Code 696, Greenbelt, MD 20771, USA.

C/NOFS observations of deep plasma depletions at dawn

Odile de La Beaujardière,[1] John M. Retterer,[1] Robert F. Pfaff,[2] Patrick A. Roddy,[1] Christopher Roth,[3] William J. Burke,[1] Yi Jiun Su,[1] Michael C. Kelley,[4] Ronald R. Ilma,[4] Gordon R. Wilson,[1] Louise C. Gentile,[1] Donald E. Hunton,[1] and David L. Cooke[1]

Received 24 April 2009; revised 11 June 2009; accepted 25 June 2009; published 7 August 2009.

[1] The Communication/Navigation Outage Forecasting System (C/NOFS) satellite was launched in 2008, during solar minimum conditions. An unexpected feature in the C/NOFS plasma density data is the presence of deep plasma depletions observed at sunrise at all satellite altitudes. Ionospheric irregularities are often embedded within these dawn depletions. Their frequencies strongly depend on longitude and season. Dawn depletions are also observed in coincident satellite passes such as DMSP and CHAMP. In one example the depletion extended 50° × 14° in the N-S and E-W directions, respectively. These depletions are caused by upward plasma drifts observed in C/NOFS and ground-based measurements. The reason for these upward drifts is still unresolved. We discuss the roles of dynamo electric fields, over-shielding, and tidal effects as sources for the reported depletions. **Citation:** de La Beaujardière, O., et al. (2009), C/NOFS observations of deep plasma depletions at dawn, *Geophys. Res. Lett.*, *36*, L00C06, doi:10.1029/2009GL038884.

1. Introduction

[2] The C/NOFS satellite was launched in April 2008 as an Air Force mission to forecast ambient plasma densities and irregularities in the equatorial ionosphere [*de La Beaujardière et al.*, 2004]. Instruments on the satellite measure electric fields, plasma characteristics, neutral winds, and the strength of scintillation-producing irregularities. The early phase of C/NOFS observations corresponds to the solar cycle minimum (F10.7 = 68). The pre-reversal enhancement in the vertical plasma drift, responsible for early-evening irregularities, rarely appears at such times. Instead, there is a high occurrence-rate of irregularities after midnight. In addition, distinctive deep plasma depletions are also observed at sunrise. This paper describes and analyzes these unexpected dawn depletions.

2. Observations of Dawn Depletions

[3] This paper focuses on data acquired by two C/NOFS sensors. The Planar Langmuir Probe (PLP) measures the ambient ionospheric densities and electron temperatures. It also provides high temporal (512 Hz) and spatial (∼13 m) resolution measurements of density irregularities. The Vector Electric Field Instrument (VEFI) measures the AC and DC electric and magnetic fields. Electric fields are measured with three orthogonal 20 m tip-to-tip booms. Initial comparisons between VEFI and PLP with observations from the Jicamarca incoherent scatter radar (ISR) showed good agreement, supporting their validity.

[4] Figure 1 provides our first example of a deep plasma depletion observed at sunrise during C/NOFS orbit #915, on June 8, 2008 at 09:34 UT, while the satellite was at 410 Km altitude. Figure 2, bottom shows ion densities at finer (1-s) temporal resolution. At the western wall of the depletion, ion density decreased by four orders of magnitude from 5.10^4 to ∼5 cm^{-3} in 30 seconds (∼200 km in track). The locations of the dawn terminator at the altitudes of the satellite (09:32 UT), and the E-layer (∼09:35 UT) are indicated. C/NOFS entered the depletion shortly before crossing the E-region terminator. Figure 2 also shows the presence of large-amplitude irregularities within the depletion. While the west wall is extremely sharp, the east side shows a gradual upward slope, due to progressive refilling of the ionosphere from below.

[5] The vertical component of the $\mathbf{V} = (\mathbf{E} \times \mathbf{B})/B^2$ plasma drift is also plotted in Figure 2. The drift turned upwards about 600 km to the west of where C/NOFS entered the depletion and remained so across it. Three large (∼200 m/s) upward spikes appear. The first occurred ∼1.3 minutes before the ion density minimum. The third is collocated with the depletion's west wall. The drifts presented in Figure 2 include the structured drifts associated with the dawn plasma cavity, and are enhanced compared to the background drift. During this period, we estimate that the peak background drift was ∼80 m/s. This value was successfully used to model the background density depletion by *Su et al.* [2009]. Although we do not understand well the cause of these enhanced drifts and their relation to the density cavity, the drifts are not large compared to upward drifts of classical spread-F depletions, which sometimes are observed with speeds of 500 m/s or even 1 km/s. Note also that the conductivities during this period are so low that high electric fields can be maintained. There is no plasma to short them out. In addition, the reported E-fields are similar to the enhanced fields observed near sunrise and reported by *Aggson et al.* [1995] (see event C of *Aggson et al.* [1995, Figure 1]).

[6] Ionosonde measurements on this day from Jicamarca corroborate the C/NOFS VEFI measurements. The low plasma density precluded using ISR measurements, but the ionosonde data can be used to estimate upward drifts.

[1]Space Vehicles Directorate, Air Force Research Laboratory, Hanscom AFB, Massachusetts, USA.
[2]NASA Goddard Space Flight Center, Greenbelt, Maryland, USA.
[3]Atmospheric and Environmental Research, Inc., Lexington, Massachusetts, USA.
[4]School of Electrical and Computer Engineering, Cornell University, Ithaca, New York, USA.

0094-8276/09/2009GL038884$05.00

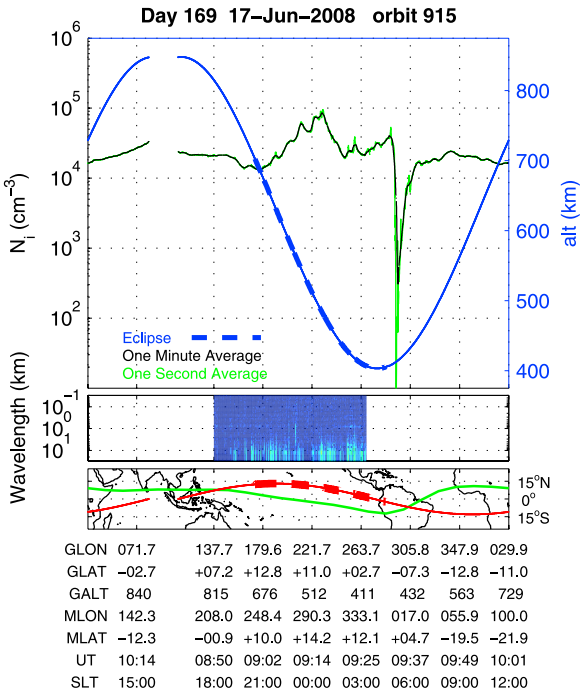

Figure 1. Dawn plasma depletion, orbit 915, Jun 17, 2008. (top) 1-min integrated ionospheric density (black), 1-s integrated density (green), satellite altitude (blue). Middle panel: FFT from the 512 Hz PLP data. (bottom) Map with satellite trajectory (red) and magnetic equator (green). Thicker dotted lines indicate when C/NOFS was in darkness.

Between 09:45 and 10:00 UT (∼05 LT), the F-layer peak altitude increased. The velocity inferred from this rise was ∼15 m/s. Then, between 10:00 and 10:05, the upward velocity abruptly increased to 125 m/s. After 10:05, it was not possible to accurately measure the F peak, because the density was too low to allow for the o-mode return to be seen. Using he x-mode return, we infer that the upward drift may have remained high, possibly reaching 50 m/s, until 10:35 UT. The ionosonde return is an average over the large region covered by the antenna beam, necessarily much lower than a point measurement from a satellite. Therefore the ionosonde data confirm the presence of large upward drifts at dawn on that day and are consistent with the C/NOFS satellite VEFI in situ measurements.

[7] Figure 3 displays ion densities sampled during a nearly simultaneous pass of the Defense Meteorological Satellite Program (DMSP) satellite F17 at 850 km near the dawn meridian. F17, a sun-synchronous satellite, crossed the magnetic equator at ∼09:24 UT, about 10 minutes before C/NOFS' first encounter with the dawn depletion. The plotted measurements show that F17 detected a latitudinally broad depletion with embedded irregularities. An examination of DMSP passes reveals that encounters with similar depletions at dawn are not unusual during this period.

[8] C/NOFS crossed similar depletions at all altitudes between perigee and apogee. Figure 4 provides a second example of a dawn plasma depletion. It occurred at 23:09 UT while the satellite was at 650 km in the Indian longitude sector. A Fast Fourier Transform (FFT) of ion densities sampled at 512 Hz, represented as color spectrograms in the middle panel, indicates that irregularities appeared within the dawn depletions but not elsewhere during this pass.

[9] This orbit was selected because CHAMP, a polar-orbiting satellite at 325 km altitude, traversed the same dawn depletion ∼20 min earlier. Figure 5a displays *in-situ* ion densities measured by CHAMP during ∼1 orbit (red line). International Reference Ionosphere (IRI) plasma densities along the CHAMP trajectory are also shown (green line) for comparison. CHAMP crossed the magnetic equator at ∼05 and 17 LT. The pronounced density minimum at the center of Figure 5a coincides with the satellite's crossing of the magnetic equator on the morning side at 22:47 UT. The density fell from 10^5 to 2×10^3 cm^{-3}. Note that IRI failed to reproduce this depletion, predicting densities well above all measured values.

[10] Figure 5b summarizes characteristics found in the present example. The depletion is located just to the west of the E-region terminator. The dimensions of this dawn depletion deduced from the roughly orthogonal C/NOFS and CHAMP orbits are 14° in longitude and 50° in latitude. The oval sketched in this map approximates the size of the depleted ionosphere, and illustrates its large extent.

[11] Almost identical dawn depletions were seen by CHAMP during seven consecutive orbits on this day. Each time, the depletion occurred as the satellite crossed the magnetic equator and very close to the E-region terminator. Electron temperatures (not shown) measured by CHAMP within these depletions were 1,000°, as predicted by IRI. Several days earlier, when the satellite's orbit was near the 06 LT meridian, electron temperatures peaked near 3100° during the equatorial crossing.

[12] Ion densities measured by CHAMP at the magnetic equator were averaged in one-hour bins, from 03 to 07 LT (L. McNamara, private communication, 2009). Morning side density depletions are deepest in the 05 LT bin. In

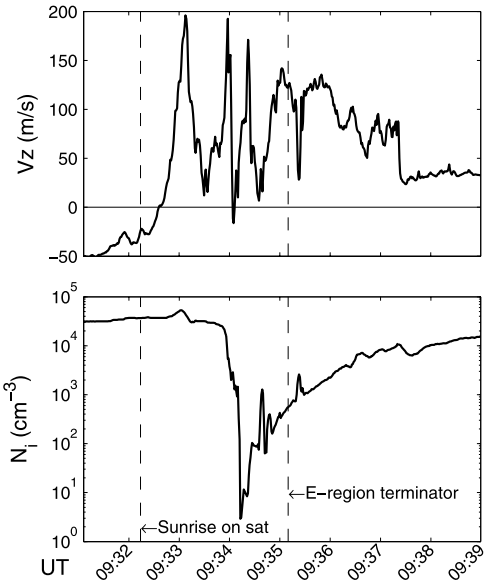

Figure 2. High time-resolution ion density and plasma drift, 17 June 2008.

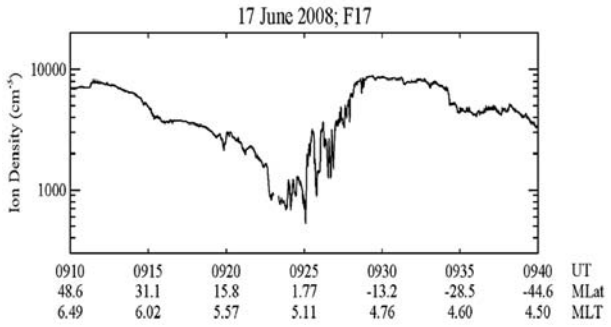

Figure 3. DMSP F17 ion density, 17 June 2008.

September 2008 they were deepest in two longitude sectors: 30° to 110°, and 310° to 350°.

3. Discussion

[13] To recapitulate, the C/NOFS satellite repeatedly observed deep plasma density depletions close to its crossings of the E-layer terminator. They are associated with irregularities and were observed at all C/NOFS altitudes (400 to 850 km). Similar depletions were crossed by the polar-orbiting DMSP and CHAMP spacecraft. Closely coincident passes of C/NOFS and DMSP/CHAMP indicate that the depletions cover about 14° in longitude and 50° in latitude.

[14] Preliminary results show that occurrence rates of these dawn depletions depend on season and longitude. For example, between September 10 and 15, 2008, dawn depletions were seen in 77% of C/NOFS passes. However, significantly fewer events were observed between November 1 and 6, 2008 when dawn depletions were recorded in only 15% of the orbits. In all seasons, depletions appear more frequently and are deeper in the America-Africa and India-Indonesia longitude sectors. The presented data were acquired during magnetically quiet times. The Kp index was 2+ and 1−, for the June and September examples, respectively, and remained low throughout the entire two days. Conditions were generally quiet from 10 to 15 Sept with Kp $\leq$ 3, except for the last 9 hours of the 15th when Kp = 4.

[15] *Scherliess and Fejer* [1999] indicate that upward plasma drifts appeared in their recorded satellite and ground data and were subsequently incorporated into their climatological model. For example, scatter plots in their Figures 1 and 2 show many instances of upward drifts in the dawn LT sector. Their plots show peaks of 20 and 40 m/s, respectively. These represent background drifts and are of similar magnitude as the C/NOFS drifts reported here. Interestingly, their Figure 4 shows large discrepancies between the model and average drift values at night after ~20:00. As indicated above, large upward drifts at dawn were also deduced from the Jicamarca ionosonde. Thus, the C/NOFS measurements are not unique in showing significant upward drifts around 05 LT.

[16] *Retterer et al.* [2005] developed the Physics Based Model (PBMod) to assist C/NOFS analysis. *Su et al.* [2009] ran PBMod twice for the entire June 17day: first, using VEFI measurements and then, using the climatological electric fields of *Scherliess and Fejer* [1999] as drivers. As mentioned above, the PBMod simulation using VEFI inputs reproduced the observed dawn density depletion. It also showed the height of maximum density H_mF_2 reaching ~900 km with well separated Appleton anomaly peaks. The climatological-driven simulation reproduced neither feature.

[17] This paper is not the first to report dawn depletions. *Burke et al.* [1979] described dawn-sector depletions observed by the DMSP F2 satellite under solar minimum conditions. However, electric fields were unavailable at that time. *Oya et al.* [1986] inferred plasma density depletions at dawn from responses of an impedance probe on the Hinotori satellite during the 1981–1982 solar maximum. ROCSAT-1 also crossed density reductions near sunrise during solar maximum storms [*Su et al.*, 2009]. *Fejer et al.* [1999] mention density depletions close to sunrise and attribute them to the stormtime disturbance-dynamo.

[18] We are now left with the challenge of explaining the presence of an eastward E field at dawn. The electric field could be generated by a dynamo mechanism driven by winds and/or gravitational drifts [*Eccles*, 2004], or could be due to over-shielding by region 2 Birkeland currents. The winds that drive the dynamo could be due to geomagnetic-disturbance dynamo or a traveling atmospheric disturbance triggered by the passage of the terminator [*Fujiwara and Miyoshi*, 2006]. Non-migrating tides in the equatorial ionosphere [*Immel et al.*, 2006] and the strength of the geomagnetic field may explain part of the longitudinal variation. If the ultimate cause is a dynamo produced by a zonal flow, then, in a way similar to the pre-reversal enhancement that occurs at dusk, we can invoke the requirement for current continuity across the discontinuity of conductivity at dawn to explain the generation of electric fields in the orthogonal direction, leading to vertical plasma drifts.

[19] Concerning the generation of these fields by geomagnetic activity, *Burke et al.* [2009] and *Su et al.* [2009]

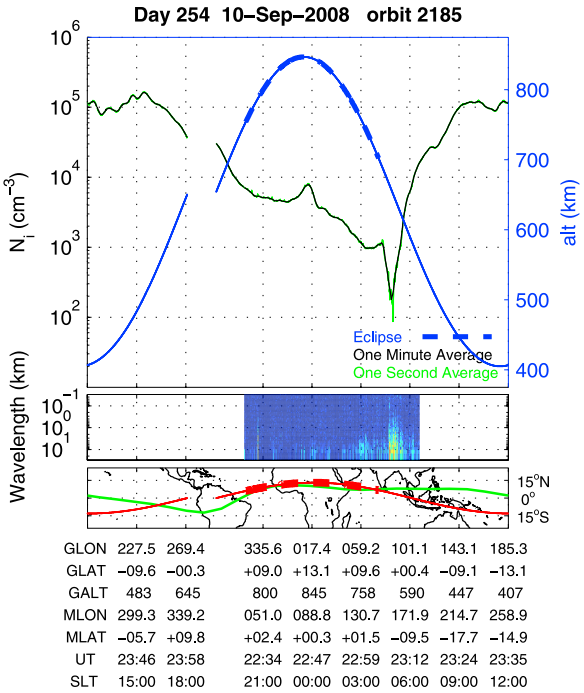

Figure 4. Same as Figure 1, but for 10 September 2008.

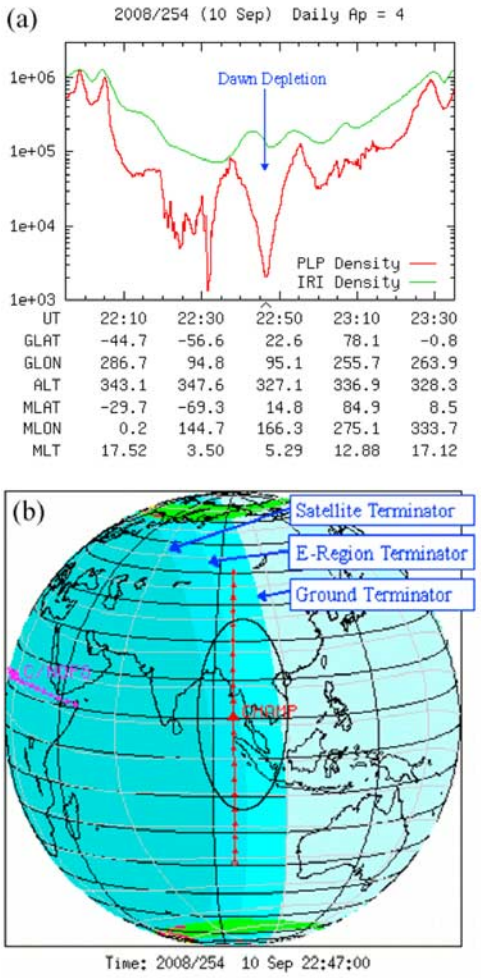

Figure 5. (a) CHAMP data, 10 September 2008 with density (red) and IRI model (green). (b) Sketch of the depleted ion density region in the dawn depletion, 10 September 2008. Both CHAMP and C/NOFS see dawn depletions when the E region below the satellite is still in darkness, but very close to the terminator. Oval illustrates the depletion size $\sim 50^\circ \times 14^\circ$.

argue that the event of June 17 may be due to the disturbance dynamo or over-shielding by Region 2 currents. A solar wind disturbance reached the Earth on June 14. Although it did not drive a magnetic storm, it did cause irregular increases in the AE index during the following days. AE reached ~700 nT at 05 UT on June 16. The authors of these two papers regard the Figure 1 depletion as a remnant of a wider depletion that had formed earlier. Nevertheless, this remnant cannot be considered a dead depletion. It was kept alive and nurtured by continuing large upward drifts. It is clear, however, that many dawn depletions observed during C/NOFS passes cannot be regarded as remnants of prior geomagnetic activity. They appear spontaneously as isolated events that start at about 05 LT, with no discernible antecedent signatures.

4. Conclusion

[20] We have shown that deep pre-sunrise depletions associated with upward plasma drifts were frequently observed by C/NOFS. Coincident DMSP and CHAMP data provide an estimate of the extent of these depletions. Using the electric field measured by VEFI, PBMod has reproduced the observed features of the depletions. We considered several possible reasons for the generation of the observed upward drifts. As part of our future work we plan to investigate in more detail possible explanations for these depletions at 05 LT. In addition, as C/NOFS measurements accumulate, we will derive statistical models of this effect in order to understand how and why the dawn depletions and corresponding E-fields vary with longitude, local time, season, magnetic activity and solar flux.

[21] **Acknowledgments.** The C/NOFS mission is supported by the Air Force Research Laboratory, the Department of Defense Space Test Program, the National Aeronautics and Space Administration (NASA), the Naval Research Laboratory, and The Aerospace Corporation. This work was also supported by the Air Force Office of Scientific Research.

References

Aggson, T. L., F. A. Herrero, J. A. Johnson, R. F. Pfaff, H. Laakso, N. C. Maynard, and J. J. Moses (1995), Satellite observations of zonal electric fields near sunrise in the equatorial ionosphere, *J. Atmos. Terr. Phys.*, *57*, 19–24, doi:10.1016/0021-9169(93)E0013-Y.

Burke, W. J., R. C. Sagalyn, R. G. Rastogi, M. Ahmed, F. J. Rich, D. E. Donatelli, and P. J. L. Wildman (1979), Postsunrise refilling of the low-latitude topside ionosphere, *J. Geophys. Res.*, *84*, 4201–4206, doi:10.1029/JA084iA08p04201.

Burke, W. J., O. de la Beaujardière, L. C. Gentile, D. E. Hunton, R. F. Pfaff, P. A. Roddy, Y.-J. Su, and G. R. Wilson (2009), C/NOFS observations of plasma density and electric field irregularities at post-midnight local times, *Geophys. Res. Lett.*, doi:10.1029/2009GL038879, in press.

de La Beaujardière, O., et al. (2004), C/NOFS: A mission to forecast scintillations, *J. Atmos. Sol. Terr. Phys.*, *66*, 1573–1591, doi:10.1016/j.jastp.2004.07.030.

Eccles, J. V. (2004), The effect of gravity and pressure in the electrodynamics of the low-latitude ionosphere, *J. Geophys. Res.*, *109*, A05304, doi:10.1029/2003JA010023.

Fejer, B. G., L. Scherliess, and E. R. de Paula (1999), Effects of the vertical plasma drift velocity on the generation and evolution of equatorial spread *F*, *J. Geophys. Res.*, *104*, 19,859–19,869, doi:10.1029/1999JA900271.

Fujiwara, H., and Y. Miyoshi (2006), Characteristics of the large-scale traveling ionospheric disturbances during geomagnetically quiet and disturbed periods simulated by a whole atmosphere general simulation model, *Geophys. Res. Lett.*, *33*, L20108, doi:10.1029/2006GL027103.

Immel, T. J., E. Sagawa, S. L. England, S. B. Henderson, M. E. Hagan, S. B. Mende, H. U. Frey, C. M. Swenson, and L. J. Paxton (2006), Control of equatorial ionospheric morphology by atmospheric tides, *Geophys. Res. Lett.*, *33*, L15108, doi:10.1029/2006GL026161.

Oya, H., T. Takahashi, and S. Watanabe (1986), Observation of low latitude ionosphere by the impedance probe on board the Hinotori satellite, *J. Geomagn. Geoelectr.*, *38*, 111.

Retterer, J. M., D. T. Decker, W. S. Borer, R. E. Daniell Jr., and B. G. Fejer (2005), Assimilative modeling of the equatorial ionosphere for scintillation forecasting: Modeling with vertical drifts, *J. Geophys. Res.*, *110*, A11307, doi:10.1029/2002JA009613.

Scherliess, L., and B. G. Fejer (1999), Radar and satellite global equatorial *F* region vertical drift model, *J. Geophys. Res.*, *104*, 6829–6842, doi:10.1029/1999JA900025.

Su, Y.-J., J. M. Retterer, O. de La Beaujardière, W. J. Burke, P. A. Roddy, R. F. Pfaff Jr., G. R. Wilson, and D. E. Hunton (2009), Assimilative modeling of equatorial plasma depletions observed by C/NOFS, *Geophys. Res. Lett.*, *36*, L00C02, doi:10.1029/2009GL038946.

W. J. Burke, D. L. Cooke, O. de La Beaujardière, L. C. Gentile, D. E. Hunton, J. M. Retterer, P. A. Roddy, Y. J. Su, and G. R. Wilson, Space Vehicles Directorate, Air Force Research Laboratory, 29 Randolph Road, Hanscom AFB, MA 01731, USA. (odile.delabeaujardiere@hanscom.af.mil)

R. R. Ilma and M. C. Kelley, School of Electrical and Computer Engineering, Cornell University, 318 Rhodes Hall, Ithaca, NY 14853, USA.

R. F. Pfaff, NASA Goddard Space Flight Center, Mail Code 674, Greenbelt, MD 20771, USA.

C. Roth, Atmospheric and Environmental Research, Inc., 131 Hartwell Avenue, Lexington, MA 02421-3136, USA.